

ABSTRACT

THE EFFECTS OF ORGANIC LIGANDS ON BIOTIC OXIDATION OF Fe(II) IN REDUCED NONTRONITE BY *PSEUDOGUBENKIANIA SP. STRAIN 2002*

by Simin Zhao

Nitrate-dependent Fe(II) oxidation (NDFO) is important for multiple environmental processes including nitrate remediation, heavy metal mobility and transport, and nuclear waste disposal. Past research has focused on microbial oxidation of either aqueous Fe²⁺ or structural Fe(II) in minerals, however, the effects of organic ligands on this process are not yet well understood, though organic ligands are ubiquitous in natural environments. The aim of this research was to study the NDFO process of structural Fe(II) in reduced nontronite (rNAu-2) by lithoautotrophic *Pseudogulbenkiania* sp. Strain 2002 in the presence oxalate (OXA) and nitrilotriacetic acid (NTA), to determine their effects on Fe(II) oxidation and mineral transformations. Bio-oxidation experiments were conducted using microbially reduced NAu-2 and nitrate as the sole electron donor and acceptor, respectively, under bicarbonate buffered neutral pH condition. A much faster rate of Fe(II) oxidation by strain 2002 than that of chemical oxidation by nitrite suggests a dominating biological role in the NDFO process. Fe(II) oxidation rate and extent were much higher in OXA and NTA groups than in no-ligand group. The ligand-promoted dissolution of rNAu-2 and the formation of highly bio-oxidizable Fe(II)-ligand complex and reduction of Fe(III)-ligand complex back to Fe(II)-ligand complex by structural Fe(II) in rNAu-2 via a process called interfacial electron transfer are the mechanisms for the enhanced oxidation rate and extent. In all biotic treatments, nitrate was predominantly reduced to N₂ with a small amount of N₂O gas and a negligible amount of nitrite. The ratio of oxidized Fe(II) to reduced nitrate was non-stoichiometric, probably resulting from heterotrophic nitrate reduction by cell-stored carbon. Structural Fe in rNAu-2 was more susceptible to chelation and liberation by organic ligands compared to unreduced NAu-2, but the structure of rNAu-2 was nearly restored to unreduced NAu-2 upon microbial oxidation in the presence of oxalate and NTA. Ferrosilite precipitated in abiotic oxalate group but not in biotic oxalate group, apparently due to oxidation of Fe(II) to Fe(III). No new minerals precipitated in NTA groups (biotic or abiotic), apparently due to its strong chelating ability. The results of this study highlight the importance of organic ligands on microbially-mediated Fe(II) oxidation kinetics and mineral transformations. These findings have important implications for iron and nitrogen biogeochemical cycles in natural environments.

THE EFFECTS OF ORGANIC LIGANDS ON BIOTIC OXIDATION OF FE(II) IN
REDUCED NONTRONITE BY *PSEUDOGUBENKIANIA SP. STRAIN 2002*

Thesis

Submitted to the

Faculty of Miami University

in partial fulfillment of

the requirements for the degree of

Master of Science

by

Simin Zhao

Miami University

Oxford, Ohio

2019

Advisor: Hailiang Dong

Reader: John Rakovan

Reader: Jonathan Levy

©2019 Simin Zhao

This Thesis titled
THE EFFECTS OF ORGANIC LIGANDS ON BIOTIC OXIDATION OF FE(II) IN
REDUCED NONTRONITE BY *PSEUDOGUBENKIANA SP. STRAIN 2002*

by

Simin Zhao

has been approved for publication by

College of Arts and Science

and

Department of Geology and Environmental Earth Science

Hailiang Dong

John Rakovan

Jonathan Levy

Table of Contents

1. INTRODUCTION.....	1
2. MATERIALS AND METHODS	5
2.1. BACTERIAL CULTIVATION	5
2.2. MINERAL, MEDIA AND EXPERIMENT SET-UP	6
2.2.1. Preparation of microbially reduced NAu-2	6
2.2.2. Preparation of organic ligands.....	6
2.2.3. Microbial oxidation of rNAu-2	7
2.2.4. Abiotic oxidation of rNAu-2 by nitrite in the presence of organic ligands.....	8
2.2.5. Organic ligand dissolution effects on unreduced NAu-2.....	8
2.2.6. Interfacial electron transfer from Fe(II) in rNAu-2 to Fe(III)-ligand complexes.....	9
2.3. ANALYTICAL METHODS.....	9
2.3.1. Measurements of Fe(II), nitrate, nitrite and N ₂ Concentrations	9
2.3.2. Fe-ligand complex measurement with ultraviolet–visible spectrophotometry and dissolved metal concentrations with inductively coupled plasma optical emission spectrometry (ICP-OES).....	10
2.3.3 FTIR and XRD	10
2.3.4. SEM.....	11
2.3.5. Biogeochemical modeling.....	12
3. RESULTS	14
3.1 MICROBIAL OXIDATION OF BIO-REDUCED NAU-2 WITH OR WITHOUT ORGANIC LIGANDS.....	14
3.1.1 Nitrate-dependent Fe(II) oxidation of rNAu-2 with or without the presence of ligands.....	14
3.1.2 Abiotic oxidation of rNAu-2 by nitrite	16
3.1.3. Spectroscopic evidence for Fe-OXA and Fe-NTA complex formation	17
3.1.4 Interfacial electron transfer between Fe(III)-ligand complexes and rNAu-2..	17
3.2 EFFECTS OF ORGANIC LIGAND ON NAU-2 DISSOLUTION.....	18
3.3 MINERALOGICAL CHANGES ASSOCIATED WITH NITRATE-DEPENDENT Fe(II) OXIDATION.....	19
3.3.1 FTIR results	19
3.3.2 XRD results	20
3.3.3 SEM observations	20
4. DISCUSSION	21
4.1 THE EFFECT OF ORGANIC LIGANDS ON MICROBIALY CATALYZED NDFO	21
4.2 ORGANIC LIGAND EFFECTS ON NAU-2 DISSOLUTION AND SECONDARY MINERAL PRECIPITATION	23
4.3 ENVIRONMENTAL IMPLICATION	24
5. CONCLUSIONS	26
REFERENCES.....	27

TABLES.....	43
FIGURES.....	44

List of Tables

Table 1. Fe(II) concentration before and after bio-oxidation, and bio-oxidation extent and rate in different cell treatment groups.

Table 2. Calculated Fe(II) speciation (Visual MINTEQ 3.1) of cell treatment groups in the presence of NTA or OXA.

Table 3. Aqueous Fe^{2+} or clay structural Fe(II) oxidation rate by Strain 2002 in NDFO

List of Figures

Figure 1. A: Strain 2002 growth curve after activation from frozen stock; B: Cell number correlation with OD 600nm absorbance.

Figure 2. Growth curve of Strain 2002 on acetate, oxalate and NTA.

Figure 3. Modeling result for time-course concentration change of: total ferrous iron dissolved in solution and from rNAu-2, nitrate, and nitrite in NDFO with and addition of Oxalate, NTA and without the addition of ligand. Figure 6. Dissolved aqueous Fe^{2+} and Total aqueous Fe in NDFO.

Figure 4. Dissolved aqueous Fe^{2+} and Total aqueous Fe in NDFO.

Figure 5. Nitrogenous gas production in NDFO for NTA, OXA, and no ligand group.

Figure 6. Chemical oxidation of Fe(II) in rNAu-2 by nitrite with addition of Oxalate, NTA and without the addition of ligand.

Figure 7. Pseudo-first-order rate constants (k) comparison between cell biotic oxidation and nitrite abiotic oxidation of Fe(II) in NAu-2.

Figure 8. Time-course UV-vis absorption spectrum of Fe-oxalate and Fe-NTA complexes.

Figure 9. Interfacial electron transfer between rNAu-2 and Fe(III)-NTA.

Figure 10. Time course (day 2, 16 to 60) change of rNAu-2 dissolved aqueous cation concentration of Fe, Si, and Mg, and Al in biotic and abiotic incubation conditions with or without OXA and NTA.

Figure 11. Aqueous Fe/Si and Al/Si ratio from rNAu-2 dissolution for OXA group and NTA group.

Figure 12. Dissolved Fe, Si, Al, Mg centration of unaltered NAu-2 under the effects of OXA and NTA.

Figure 13. FTIR spectra of OH-stretching and OH-bending bands comparison between unaltered, bio-reduced, bio-oxidized, and bio-reduced NAu-2 +organic matter abiotic group.

Figure 14. X-ray diffraction patterns of NAu-2 for unaltered, reduced and re-oxidized NAu-2 samples with or without the presence of NTA and OXA through incubation for 60 days.

Figure 15. X-ray diffraction patterns for neoformed mineral in abiotic OXA group.

Figure 16. SEM images of Strain 2002 after NAu-2 incubation for 60 days in OXA, NTA and no-ligand group.

Figure 17. Scanning electron microscopic (SEM) images and energy dispersive spectroscopy (EDS) spectrum of newly formed mineral in abiotic and biotic OXA group.

Figure 18. Conceptual model for interfacial electron transfer.

Acknowledgements

I am grateful to my advisor Dr. Hailiang Dong for his guidance and help throughout this research project and during my master's program. I'd like to thank Dr. Jonathan Levy and Dr. John Rakovan for their valuable suggestions and comments on improving the quality of this manuscript. I thank members of the Geomicrobiology research group, Miami University, for teaching me lab protocols. I'd like to thank Mr. Matt Duley, and Dr. Richard Edelmann, Center for Advanced Microscopy and Imaging (CAMI), Miami University for assistance in light microscopy and scanning electron microscopy. I thank friends, fellow graduate students, and colleagues in Department of Geology and Earth Environmental Science for their support and for a vibrant atmosphere.

Special thanks to my boyfriend Jiayan Zhao (Tony), my parents, and family members for their understanding, ceaseless love and unconditional support.

1. INTRODUCTION

Iron-bearing clay minerals are widely distributed in soils, sediments, and sedimentary rocks (Petschick et al., 1996; Stucki and Kostka, 2006; Ito et al., 2017). The redox state of structural Fe in clay minerals can be cycled either chemically or biologically (Ernstsen et al., 1998; Jaisi et al., 2005; Stucki and Kostka, 2006; Dong et al., 2009). The redox-activated iron-bearing clay minerals can potentially be applied for environmental remediation of many contaminants such as nitrate, (Ernstsen et al., 1996; Zhao et al., 2013, 2015, 2017), chromium (Michael et al., 2014; Liu et al., 2018), and uranium (Zhang et al., 2009).

In contrast to a large body of literature on microbial reduction of structural Fe(III) in clay minerals by dissimilatory iron reducing bacteria (DIRB) (Kostka et al., 1996, 1999; Kim and Dong 2004; Jaisi et al., 2007; Dong et al., 2009; Dong 2012; Liu et al., 2017; Burton et al., 2018), studies on microbially catalyzed Fe(II) oxidation are still limited. Previous research on microbial oxidation of Fe(II) has mainly focused on aqueous Fe²⁺ and iron oxides (Weber et al., 2006a; Picardal 2012; Melton et al., 2014; Bryce et al., 2018; Chen et al., 2018, Jamieson et al., 2018; Liu et al., 2018); but a few recent studies have reported microbial oxidation of structural Fe(II) in clay minerals including biotite (Shelobolina et al., 2012a); smectite and illite (Shelebolina et al., 2012b; Zhao et al., 2013, 2015, 2017; Xiong et al., 2015). The microbes that are actively involved in Fe(II) oxidation in circumneutral pH environments are mainly microaerophilic Fe(II)-oxidizing bacteria, anaerobic phototrophic Fe(II)-oxidizing bacteria, and nitrate-dependent Fe(II)-oxidizing (NDFO) bacteria (Straub et al., 1996; Weber et al., 2001; Kappler et al., 2004; Emerson et al., 2010; Hedrich et al., 2011; Lin et al., 2012; He et al., 2016; Laufer et al., 2017). Without requirement for light, NDFO microbes are more abundant than phototrophic Fe(II)-oxidizing bacteria under anoxic conditions (Kappler and Straub 2005), and they play important roles in coupled Fe and N biogeochemical cycles, which has attracted extensive research interest over the last decade, mostly using aqueous Fe²⁺ or iron oxides.

Microbial communities catalyzing the NDFO process are found in various environments such as rice paddy soils, aquifers, and marine, brackish or freshwater sediments (Straub et al., 1996; Weber et al., 2006a; Li et al. 2016; Scholz et al., 2016). With nitrate as electron acceptor, NDFO bacteria can gain energy to support cell growth through the following reaction (Straub et al., 1996; Weber et al., 2001, 2006b; Kappler et al., 2005) : $10\text{Fe}^{2+} + 2\text{NO}_3^- + 24\text{H}_2\text{O} \rightarrow 10\text{Fe}(\text{OH})_3 + 18\text{H}^+ + \text{N}_2$ (1). In this process, nitrate is usually reduced to nitrogenous gas, with nitrite as an intermediate product (Kappler et al., 2005; Weber et al., 2006b, Liu et al., 2018), whereas iron, in forms of aqueous Fe^{2+} and structural Fe(II) in Fe oxides or Fe-bearing clay minerals, can be oxidized to Fe(III), forming secondary iron minerals like goethite (Klueglein et al. 2014), lepidocrocite (Chen et al., 2018), vivianite (Zhao. et al., 2013), ferrihydrites, magnetite and green rust (Pantke et al. 2011). The secondary minerals formed are dependent on microbial strains, geochemical conditions, and Fe(II) forms (aqueous, oxide or clay minerals). For NDFO, most functional bacteria are mixotrophic (Bryce et al., 2018) and they require an organic co-substrate such as acetate to sustain Fe(II) oxidation and nitrate reduction. Such organisms include *Acidovorax* sp. strain BoFeN1 (Kappler et al., 2005), *Acidovorax ebreus* strain TPSY (Byrne-Bailey et al., 2010), *Acidovorax* sp. strain 2AN (Chakraborty et al., 2011), and *Pseudogulbenkiania* sp. strain MAI-1 (Kopf et al., 2013). To date, only a few strains, including *Pseudogulbenkiania* sp. strain 2002 (Weber et al., 2006b) and an enrichment culture KS (Straub et al., 1996) are reported to be capable of CO_2 fixation and NDFO under lithoautotrophic conditions with Fe(II) as the sole electron donor and nitrate as the sole electron acceptor. Strain 2002 (Shelebolina et al., 2012b; Zhao et al., 2013, 2015, 2017) and enrichment culture KS (Xiong et al., 2015) have been proven to be capable of oxidizing structural Fe(II) in clay minerals.

In nature Fe can form complexes with organic ligands (Fe-ligand) and natural organic matter (Fe-OM) (Perdue et al., 1976; Luther et al., 1996; Jansen et al., 2003; Hopwood et al., 2015), which may alter the kinetics of NDFO. Organic matter can be excreted by microbes, e.g. siderophore (Neilands et al., 1981), and root exudes (Fox et al., 1990; Jones et al., 1998). Organic acids can also be derived from sediments (Luther et al., 1992) and synthetic sources such as nitrilotriacetic acid (NTA) used for bioremediation of petroleum contaminated aquifers (Lovley et al., 1994) and for

decontamination of heavy metals at DOE sites (Bucheli-Witschel et al., 2001). Past studies have shown that Fe complexation with OM can affect Fe speciation, reactivity, and distribution (Taillefert et al., 2000; Jansen et al., 2003; Sharma et al., 2010; Vindedahl et al., 2016; Scholz et al., 2016; Gröhlich et al., 2017). To better understand NDFO in nature, it is therefore important to study Fe(II) oxidation kinetics and mineral transformations in the presence of ligands.

The effect of individual organic matter on NDFO has been explored for aqueous Fe²⁺. Fe(II)-ligand complexes, for instance Fe(II)-NTA, can be oxidized by various NDFO strains including *Acidovorax ebreus* strain TPSY, *Pseudogulbenkiania* strain 2002 and *Pseudogulbenkiania* sp. strain MAI-1 (Weber et al., 2006b; Carlson et al., 2013; Kopf et al., 2013). Fe(II)-EDTA can be oxidized by *Dechloromonas* strain UWNR4, BoFeN1, *Microbacterium* sp. W5, *Pseudogulbenkiania* strain 2002 and *Thiobacillusdenitrificans* (Chakraborty et al., 2013; Klueglein et al., 2015; Zhou et al., 2016; Kiskira et al., 2017). While NTA and EDTA can enhance Fe²⁺ oxidation process through prevention of cell encrustation and maintenance of cell viability by forming soluble Fe(III)-ligand products, Fe(II)-EDTA may be toxic to BoFeN1 and *Pseudogulbenkiania* strain 2002, as these two strains showed retarded cell growth and decreased nitrate reduction capacity in the presence of EDTA (Klueglein et al., 2015; Kiskira et al., 2017). Contrary to Fe(II)-NTA and Fe(II)-EDTA complexes, other Fe-OM complexes such as Fe-fulvic acid and Fe-humic acid decreased oxidation rate by, possibly because these large Fe-OM complexes cannot enter the periplasm for enzymatic oxidation (Peng et al., 2018). Consistent with this explanation, Pahokee Peat Humic Acid (PPHA) showed an inhibitory effect on Fe(II) oxidation by *Pseudogulbenkiania* sp. strain MAI-1, but small ligand such as citrate showed an enhancement (Kopf et al., 2013). The effect of ligand on NDFO kinetics is further complicated by the possibility of abiotic oxidation of Fe(II)-ligand complexes by nitrite, which may contribute to a significant fraction of iron oxidation in NDFO (Kopf et al., 2013). However, Carlson et al. (2013) reported that oxidation of Fe(II)-NTA by *Acidovorax ebreus* TPSY is a microbially catalyzed process. These observations suggest that the effects of organic matter on Fe(II) oxidation rate and extent, and the role of nitrite-induced abiotic oxidation of Fe(II) may be strain-specific.

Despite a few recent studies on the role of OM in microbial oxidation of aqueous Fe^{2+} , the effect of OM on microbial oxidation of structural Fe(II) in clay minerals has not yet been studied, even though OM commonly coexists with clay minerals in natural environments (Lovely et al., 1986; Kahle et al., 2004; Lehmann et al., 2015). This knowledge gap is in contrast to extensive studies of the OM effects on bioreduction of Fe(III)-bearing oxides and clay minerals (Arnold et al., 1988; Lovely et al., 1996; Urrutia et al., 1999; Royers et al., 2002a, b; Liu et al., 2017; Stern et al., 2018). In these studies, natural organic matter (Royers et al., 2002a, b), humic substances (Liu et al., 2017; Stern et al., 2018), NTA (Arnold et al., 1988; Urrutia et al., 1999; Lovely et al., 1996), oxalate and citrate (Kostka et al., 1999), and malate (Urrutia et al., 1999), were observed to enhance bio-reduction of Fe(III) in Fe-bearing minerals like Fe oxides and clay minerals. Mechanisms for such enhancements include: 1) chelation that solubilizes Fe(III) from Fe-bearing minerals to form soluble Fe(III)-complexes, which are more susceptible to microbial reduction (Lovley et al., 1996; Koska et al., 1999; Parrello et al., 2016; Liu et al., 2017); 2) electron shuttling to enhance Fe(III) reduction (Royers et al., 2002a,b; Liu et al., 2017; Stern et al., 2018); 3) formation of soluble Fe(II) products that prevents Fe(II) sorption onto mineral and cell surfaces and thus removes the inhibitory effect (Urrutia et al., 1999). However, equivalent research has not been studied for microbial oxidation of structural Fe(II) in clay minerals in the presence of ligands. It remains unclear if similar mechanisms operate for NDFO of clay minerals.

The objective of this study is therefore to fill the above knowledge gap by studying nitrate-dependent oxidation of structural Fe(II) in a microbially reduced iron-rich smectite, nontronite (rNAu-2) by nitrate-dependent Fe(II) oxidizer *Pseudogulbenkiania* strain 2002 with or without the presence of oxalate (OXA) and NTA, two representative model ligands. Specifically, we aim to study the effect of oxalate and NTA on: 1) the rate and extent of Fe(II) oxidation and nitrate reduction; 2) mineralogical changes associated with NDFO. Based on the known effects of OM on bioreduction of structural Fe(III) in clay minerals and on microbial oxidation of aqueous Fe^{2+} , we hypothesize that Fe(II) oxidation rate and extent of rNAu-2 in NDFO will be enhanced in the presence of OXA and NTA. Wet chemistry was used to measure the kinetics of Fe(II) oxidation and nitrate reduction, which was fitted with a kinetic rate

model. UV-visible spectroscopy was used to measure Fe(II)-ligand complex formation. Fourier-transform infrared spectroscopy (FTIR), X-ray diffraction (XRD), and electron microscopy were used to determine mineralogical transformations. The results of this study highlight the importance of organic ligands on the NDFO kinetics and mineral transformation.

2. MATERIALS AND METHODS

2.1. Bacterial cultivation

Pseudogulbenkiania sp. strain 2002 was isolated by most-probable-number enumeration under nitrate-dependent Fe(II)-oxidizing condition (Weber et al., 2006b). Strain 2002 is an anaerobic betaproteobacterium capable of heterotrophic growth with organic substrate as electron donor and nitrate as electron acceptor, or litho-autotrophic growth with Fe(II) as electron donor and nitrate as electron acceptor (Weber et al., 2006b, 2009). Strain 2002 is routinely cultured in anoxic freshwater basal medium with sodium acetate (10mM) and sodium nitrate (10 mM) as electron donor and acceptor, respectively in the presence of vitamins and trace minerals (Weber et al., 2009). Prior to experiment, frozen stock of strain 2002 was activated for 24 hours, and then transferred to a new growth medium. Cell growth was periodically monitored by turbidity measurement at OD 600 nm on a spectrophotometer (Figure 1A). When reaching the log phase, cells were harvested and washed three times with repeated centrifugation (6000 g, 10min) and resuspension with anoxic (80:20 N₂: CO₂ purged) bicarbonate buffer (29.76 mM NaHCO₃ and 1.34 mM KCl at pH 7.0) to remove acetate and nitrate. After the final wash, cells were resuspended in the same bicarbonate buffer to serve as a stock. The stock cell concentration was checked through direct cell counts (Petroff-Hausser counting chamber, 0.02-mm depth), and once a correlation between optical density at 600 nm (OD600) and cell count was established (Figure 1B, R²=0.9984), OD was used in subsequent experiments as a proxy for cell counts.

2.2. Mineral, Media and Experiment Set-up

2.2.1. Preparation of microbially reduced NAu-2

Nontronite (NAu-2), purchased from the Clay Minerals Society, has a formula of $M_{0.72}(Si_{7.55}Al_{0.45})(Fe_{3.83}Mg_{0.05})O_{20}(OH)_4$, where M represents interlayer cations such as K, Ca, and Na. The Fe content of NAu-2 was 24%, of which 92% was in octahedral site and 8% in tetrahedral site (Keeling et al., 2000; Gates et al., 2002). The NAu-2 sample was size fractionated to obtain a size range of 0.02-0.5 μ m (Liu et al., 2011). NAu-2 (5 g/L) was suspended in bicarbonate buffer, purged with N_2/CO_2 (80:20), and autoclaved.

Bio-reduction of structural Fe(III) in NAu-2 was achieved using *Shewanella putrefaciens* CN32 with lactate (10 mM) as electron donor, structural Fe(III) in NAu-2 as electron acceptor, and anthraquinone-2,6-disulfonate (AQDS) (0.1 mM) as electron shuttle at 30°C (Jaisi et al., 2007; Zhao et al., 2013). When the Fe(III) reduction extent reached 23%, the reduction vials were pasteurized (one time at 80°C for 3 hrs) to stop the reaction (Jasi et al., 2008). The reduced NAu-2 (hereafter called rNAu-2) was washed with repeated centrifugation and resuspension to remove lactate, AQDS and CN32 cells. The washed rNAu-2 was re-suspended in the same buffer, adjusted to a final pH of 6.8-7.0 with anoxic sterile HCl or NaOH, and pasteurized, e.g., three rounds of hot (80°C 1 hr) and cold (4°C 0.5 hr) water bath (Zhao et al., 2013; 2015). The sterilization of rNAu-2 stock solution was confirmed by lack of growth of CN32 cells on agar plates.

2.2.2. Preparation of organic ligands

Oxalate (OXA) is commonly present in the rhizosphere soil (Jones et al., 1988), and Nitritotriacetic acid (NTA) as a synthetic OM is frequently used in decontamination sites such as DOE Hanford site. NTA is also widely used in daily products such as detergent and cleanser, and it is present in surface water, groundwater, and soils (Bott et al., 1980). Therefore, these two ligands were chosen as representatives to study their effect on NDFO. NTA and OXA powders were purchased from Sigma. These two powders were suspended with Milli-Q water to stock solution, wrapped with aluminum foil to prevent light degradation, adjusted pH to 7 with NaOH, purged with N_2 (100%, 30

minutes) to get anaerobic solution, and crimp-sealed with blue rubber stoppers and aluminum cap. The solution was then transferred to an anaerobic chamber (Coy Laboratory Products, Grass Lake, Michigan) and filter-sterilized.

To rule out the possibility that these two ligands may be used as growth substrate by strain 2002, a cultivation experiment was pre-performed through inoculation of strain 2002 cells with different organic substrates including: oxalate, NTA, and acetate in a freshwater basal medium in the presence of nitrate, vitamins, and trace minerals (Weber et al., 2009). Results showed that strain 2002 cannot use oxalate or NTA as a growth substrate (Figure S1), and thus NTA and OXA were used for subsequent NDFO experiment.

2.2.3. Microbial oxidation of rNAu-2

Balch tubes (25 mL) containing 6 mL bicarbonate buffer were purged, sealed, and autoclaved. After sterilization, these tubes were transferred to an anaerobic chamber and sterilized rNAu-2 stock solution was added to achieve a final concentration of ~5 g/L rNAu-2 (containing structural Fe(II) ~4.9-5 mM) as the sole electron donor, amended with anoxic and sterilized sodium nitrate as the sole electron acceptor (~10 mM final conc.). Vitamins and trace minerals were omitted to maintain a non-growth condition (Weber et al., 2006b).

Two separate experimental groups were set up to examine the effect of NTA and OXA. A small amount of NTA or OXA stock solution was added to separate tubes to achieve a final concentration of 5 mM. Finally, cell stock suspension was added to achieve a final cell concentration of $\sim 3 \times 10^8$ cell/mL. Two biotic groups were set up: Fe(II) + Cells + NO_3^- + NTA and Fe(II) + Cells + NO_3^- + OXA. The no-ligand control group was identical to experimental treatments but without any ligand: Fe(II) + Cells + NO_3^- . Two abiotic controls were set up for each ligand: Fe(II) + NO_3^- + NTA, Fe(II) + Cells (heat killed) + NO_3^- + NTA; Fe(II) + NO_3^- + OXA, Fe(II) + Cells (heat killed) + NO_3^- + OXA. For N_2 gas measurement, separate experiments were set up, where the headspace of each tube was purged with helium for 15 minutes using sterile needles right after cell inoculation. Because all control and experimental groups were amended with NO_3^- , in later descriptions NO_3^- was omitted for succinctness. For heat-killed (HK)

controls, a separate aliquot of cells (again at $\sim 3 \times 10^8$ cell/mL) was killed by heating at 121°C for 30 minutes, cooled to room temperature, and then added to the tubes. The total volume for each treatment solution was ~ 10 mL. All groups were conducted in duplicates and were incubated in an anaerobic chamber at 30°C with no light exposure (aluminum foil wrapped). The pH for each group was recorded at the end of the experiment (60 days).

2.2.4. Abiotic oxidation of rNAu-2 by nitrite in the presence of organic ligands

To rule out the possibility that some amount of nitrite could have been produced, which can chemically oxidize Fe(II) in the NDFO process, a supplementary experiment was set up to examine such chemical reaction. Sterilized rNAu-2 (final conc. 5 mM) was used as electron donor and sterilized nitrite (NaNO_2 , final concentration 2 mM) as electron acceptor under bicarbonate buffered condition in 25-mL Balch tubes: rNAu-2 + NO_2^- + OXA (5 mM), rNAu-2 + NO_2^- + NTA (5 mM), and rNAu-2 + NO_2^- . Nitrite of 2 mM in concentration was used because about 2 mM nitrate was consumed in the biotic groups in the first two days and no more than 2 mM nitrite should have been produced. Nitrite, structural Fe(II), and dissolved Fe^{2+} concentrations were monitored with the sulfanilamide method, 1,10-phenanthroline method and revised Ferrozine method, respectively, as described below.

2.2.5. Organic ligand dissolution effects on unreduced NAu-2

Because we observed more dissolution of rNAu-2 (by NTA and OXA) in abiotic groups than in cell-added groups, we hypothesized that bio-oxidation of rNAu-2 stabilized the structure and resulted in less dissolution. To test this hypothesis, a supplementary experiment was performed, where a sterile and anoxic NAu-2 solution (99.4% of Fe was Fe(III), 5 g/L) was mixed with anoxic OXA (5 mM) or NTA (5 mM) and NaNO_3^- (10 mM) for 16 days. The dissolved cations (Fe, Si, Mg, and Al) were measured with inductively-couple plasma optical emission spectrometry (ICP-OES) as described below.

2.2.6. Interfacial electron transfer from Fe(II) in rNAu-2 to Fe(III)-ligand complexes

Because we observed partial dissolution of rNAu-2, Fe-ligand complexation, and a much faster Fe(II) oxidation rate in the OXA and NTA groups than in the no-ligand group, we proposed that OXA and NTA dissolved rNAu-2, released Fe(II) and Fe(III) formed complexes with these ligands, and Fe(II)-ligand complexes were then bio-oxidized to Fe(III)-ligand complexes by strain 2002 via NDFO. The resulting Fe(III)-ligand complexes may receive electrons from structural Fe(II) in rNAu-2 via a process similar to interfacial electron transfer (IET), but in a reversed direction. To test this hypothesis, a supplementary experiment was designed by mixing 0.9 mM Fe(III)-NTA complex (1:1 FeCl₃ - NTA ratio, pH 7) with rNAu-2 [pH 7, 4.8 mM Fe(II)]. To test the electron-donating capacity of rNAu-2, once the production of aqueous Fe²⁺ stopped, a fresh spike of Fe(III)-NTA was added until there was no more reduction of Fe(III)-NTA upon addition of a new spike. Structural Fe(II) in rNAu-2, aqueous Fe²⁺, and total aqueous Fe concentration were monitored with 1,10-penanthroline and Ferrozine methods as described below.

2.3. Analytical Methods

2.3.1. Measurements of Fe(II), nitrate, nitrite and N₂ Concentrations

The reaction progress was monitored by measuring time-course change of concentrations of clay-associated Fe(II), dissolved Fe²⁺, clay-associated total Fe, dissolved total Fe, nitrate, and nitrite. Clay-associated Fe(II) was measured on the clay solid. To prevent chemical oxidation of Fe(II) by nitrite under acidic boiling condition used in this method, supernatant was separated from the solid via centrifugation at 10,000 x g for 10 minutes. The clay pellet was washed three times with anoxic and sterile bicarbonate buffer (Zhao et al., 2015) and resuspended for 1,10-penanthroline measurement (Amonette and Templeton, 1998). To measure aqueous Fe²⁺ and aqueous total Fe, samples were collected from the supernatant and were measured with a revised ferrozine method using sulfamic acid treatment to remove nitrite before complexation of Fe²⁺ with Ferrozine (Schaedler et al., 2017). Total aqueous Fe was measured with the

revised Ferrozine method once Fe^{3+} was reduced to Fe^{2+} by hydroxylamine hydrochloride. Concentrations of nitrate and nitrite in the supernatant were determined with a diazotization method using sulfanilamide under acidic condition. The measurement was made with a Lachat Quickchem 8500 Series ii Flow Injection Analysis System (Instruments et al., 2000). Headspace N_2 gas was measured with an Agilent 7890A Gas Chromatographic (GC) system.

2.3.2. Fe-ligand complex measurement with ultraviolet–visible spectrophotometry and dissolved metal concentrations with inductively coupled plasma optical emission spectrometry (ICP-OES)

NTA and oxalate are strong chelates that can dissolve clay minerals to form NTA- and OXA-complexes (Kostka et al., 1999; He et al., 2011), and thus may affect the kinetics of NDFO. Fe-NTA and Fe-OXA complex formation was examined over time (2, 16, and 60 days) with ultraviolet–visible spectrophotometry (UV-vis) (Pozdnyakov et al., 2008; De et al., 2015). Fresh samples were extracted with 1 mL sterile syringe and centrifuged (10,000 x g, 10 minutes). The supernatant was filtered through a 0.22 μm nylon filter. Absorption spectra with a scan range of 200 nm–800 nm were recorded using a model 1050 high-performance lambda spectrophotometer (Perkin Elmer, Waltham, Massachusetts).

To monitor any ligand-induced NAu-2 and rNAu-2 dissolution, clay suspensions were filtered and fixed in 2% nitric acid (final conc.). Dissolved cations (Fe, Si, Mg, and Al) in the filtrate were measured over the same time duration (60 days) with ICP-OES (Agilent 5110 ICP-OES at the STAR lab, Ohio State University, USA).

2.3.3 FTIR and XRD

Structural changes of NAu-2 upon bio-reduction and bio-oxidation with or without organic ligands were examined using attenuated total reflection infrared spectroscopy (ATR-FTIR). NAu-2 suspension was collected from the reaction tubes and centrifuged (10,000 x g, 15 minutes). The supernatant was removed, and the pellet was dried at 30°C in an anaerobic chamber incubator. Approximately 2 mg of the dried NAu-2 pellet was prepared for ATR and analyzed utilizing a Spectrum 100 Frontier Infrared

Spectrometer (Perkin-Elmer, Waltham, Massachusetts). The spectra were scanned by accumulating 4 scans at 1 cm^{-1} resolution in the mid-IR range (Frost et al., 2002, Zhao et al., 2015).

At the end of the experiment, mineralogical transformations as a result of microbial oxidation of Fe(II) in the presence of NTA and OXA were studied with powder X-ray diffraction (XRD). Clay suspension was centrifuged and washed three times to make a smear amount to a petrographic slide followed by drying in a 30°C incubator inside an anaerobic chamber. The dried slide was ethylene-glycolated in a desiccator overnight until XRD analysis (Moore and Reynolds, 1997) to distinguish expandable nontronite from non-expandable clay mineral such as illite. Powder X-ray patterns were collected using a Scintag X-ray powder diffractometer with $\text{CuK}\alpha$ radiation. The sample was scanned with a step size of 0.02 and speed of 0.6° per minute for a 2-theta range of 2° to 70° , but XRD patterns up to 40° two-theta were shown because major diffraction peaks were present within this range. Burker's Diffrac. Eva software was used to identify mineral phases. The software uses the PDF2-1992 database as a reference source.

2.3.4. SEM

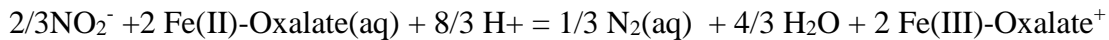
At the end of the experiment, cell-rNAu-2 associations and newly formed minerals were observed with scanning electron microscopy (SEM). After fixation with 2.5% glutaraldehyde and 2% paraformaldehyde, clay suspensions were mounted onto a poly-L-lysine pretreated cover slide for 10 minutes, followed by a series of ethanol dehydration, and critical point drying with a Tousimis Samdro-780A Critical Point Dryer (CPD) (Dong et al., 2003). The cover slips were subsequently mounted to SEM stubs with clear double-sided sticky tape and gold-coated. SEM observations were made with a Zeiss Supra 35 variable pressure (VP) SEM equipped with EDAX Genesis 2000 X-ray energy dispersive spectroscopy (SEM/EDS). The chemical composition of clay mineral was obtained using EDS with a 7-10 keV accelerating voltage and 8-10 mm working distance.

2.3.5. Biogeochemical modeling

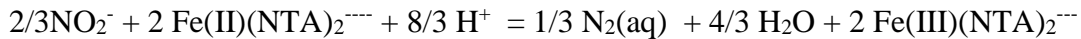
The Fe complex species were calculated with Visual MINTEQ3.1 software. The progress of the experiments was simulated using the React program of the Geochemist's Workbench software package and the Minteq thermodynamic dataset (Bethke, 2008). We amended the dataset by including rNAu-2 (see Supplementary Information). We first simulated the abiotic oxidation of Fe(II) in rNAu-2 by nitrite, and considered the following reactions:



In the presence OXA, we considered the oxidation of oxalate-Fe(II) complex,



In the presence of NTA, we considered the oxidation of NTA-Fe(II) complex,

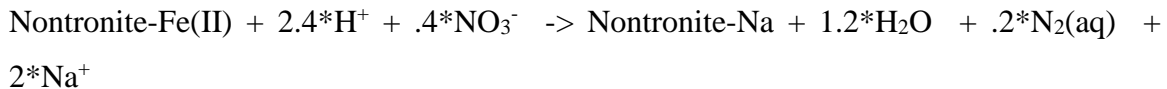


We computed the rates of Fe(II) oxidation using the first-order rate equation,

$$r = k_{\text{Fe}} \cdot m_{\text{Fe(II)}}, \quad (1)$$

where k_{Fe} is the rate constant (s^{-1}) and $m_{\text{Fe(II)}}$ the concentration of ferrous iron. We estimated the k_{Fe} value by fitting the modeling results to the laboratory observations.

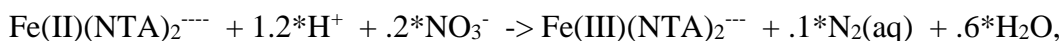
To simulate microbial Fe(II) oxidation with ligands, we described microbial Fe(II) oxidation and nitrate reduction as a kinetic process:



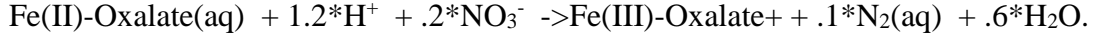
In the presence of NTA and oxalate, we assume the Fe(II) oxidation as a 3-step process:

1) partial dissolution of rNAu-2, release of Fe(II), and formation of Fe(II)-ligand complex. This is an initiator step; 2) biotic oxidation of Fe(II)-ligand by nitrate to Fe(III)-ligand complex; 3) reduction of Fe(III)-ligand complex back to Fe(II)-ligand complex by structural Fe(II) in rNAu-2. Steps 2 and 3 repeat until the reduction capacity of rNAu-2 is exhausted. Our independent control experiment showed that step 3 is extremely fast. Thus, we assume the rate limiting step is step 2.

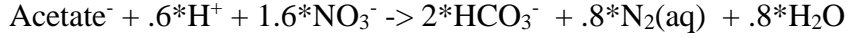
Therefore, the oxidation of NTA-Fe(II) by nitrate can be written as:



or the oxidation of Oxalate-Fe(II):



In addition, we also considered the oxidation of endogenous organic carbon coupled to nitrate reduction:



Due to the lack of identity of cellular organic carbon, we use acetate as an electron donor for nitrate reduction, but this assumption does not affect the rate calculation.

We computed the rate r of microbial reaction using the modified Monod equation,

$$r = \alpha \cdot V_{\max} \cdot m_D \cdot \frac{m_A}{m_A + K_A} \quad (2)$$

where V_{\max} is the maximum rate (s^{-1}), α is a factor that accounts for the extent of Fe(II) oxidation, $[X]$ is biomass concentration in gram dry weight per kg water ($\text{g} \cdot \text{kg}^{-1}$), m_D is the concentration of Fe(II) or endogenous organic carbon, and m_A and K_A are the concentrations of nitrate and the half-saturation constant, respectively. We evaluated the impact of Fe(II) oxidation extent according to

$$\alpha = 1 - \frac{f_{\text{Fe(III)}}}{f_o} \quad (3)$$

where $f_{\text{Fe(III)}}$ is the fraction of solid-phase Fe(III) in the total solid-phase iron (Fe(II) and Fe(III)), and f_o is the threshold fraction where iron oxidation ceases, presumably due to the blockage of electron transfer channels by the formation of Fe(III) in the mineral. We do not consider the extent in organic matter oxidation (i.e., $\alpha = 1$). We also ignore cell growth, due to the relatively large biomass provided at the beginning of the experiments. We set the K_A value of $2.3 \mu\text{M}$ (Jin and Roden, 2011) and estimate the V_{\max} value by fitting the modeling results to laboratory observations.

3. RESULTS

3.1 Microbial oxidation of bio-reduced rNAu-2 with or without organic ligands

3.1.1 Nitrate-dependent Fe(II) oxidation of rNAu-2 with or without the presence of ligands

Throughout the experimental duration (60 days), the pH remained in the range of 6.8-7.0 in all control and experimental groups. In the absence of ligands, abiotic controls in our previous studies did not show any Fe(II) oxidation or nitrate reduction, thus, we do not consider abiotic groups in the no ligand group (Zhao et al., 2013, 2015, 2017). In the presence of live cells, the oxidation of structural Fe(II) in rNAu-2 (Fig. 3a) was coupled with reduction of nitrate (Fig. 3b). Structural Fe(II) in rNAu-2 was rapidly oxidized in the first day at a rate of 0.31 mM/d followed by a slow oxidation rate until the end of the experiment (Fig. 3c). When nitrate reduction slowed, there was abundant Fe(II) remaining, and therefore, a second spike of nitrate was added on day 16. The results showed that nitrate reduction and Fe(II) oxidation slightly continued. The ultimate extent of Fe(II) oxidation, from two spikes of nitrate, reached 48% (Table 1), consistent with our earlier studies (Zhao et al., 2013, 2015). Negligible amounts of soluble Fe²⁺ and soluble total Fe were observed (Fig. 4A), suggesting that Fe(II) oxidation might have occurred in solid state. The ratio of the amount of nitrate reduction to the amount of Fe(II) oxidized was much greater (1.9) than the stoichiometric ratio of 0.2 according to equation 1. Such high ratios have been observed before (Zhao et al., 2013, 2015, 2017; Chen et al., 2018, Liu et al., 2018) and can be ascribed to extra nitrate reduction by cellular carbon stored in the cytoplasm. According to our modeling results, nitrate reduction by the oxidation of endogenous organic carbon accounted for 79% of the total nitrate reduction.

Abiotic or heat-killed OXA groups did not exhibit any Fe(II) oxidation (Fig. 3d) or nitrate reduction (Fig. 3e). Abiotic or heat-killed cell controls showed similar concentrations of soluble Fe²⁺ and soluble total Fe (Fig. 4A), suggesting that aqueous Fe²⁺ was derived from rNAu-2 dissolution and soluble Fe³⁺ was negligible. A time-course decrease in soluble Fe²⁺ (from 0.75 to 0.2 mM) was likely due to precipitation of Fe²⁺-

bearing mineral or sorption of Fe^{2+} to rNAu-2. In the live cell experiments, the presence of OXA greatly accelerated Fe(II) oxidation. In the OXA + cells treatment, Fe(II) was rapidly oxidized in the first day followed by a slow oxidation to the end of the experiment (Figs. 3d & f). Again, addition of a second spike of nitrate slightly promoted continued Fe(II) oxidation. A total of 83% (Table 1) structural Fe(II) initially present in rNAu-2 was oxidized. According to the modeling results, 96% of the Fe(II) in rNAu-2 was oxidized by microbes and the remaining Fe(II) (4%) was oxidized by nitrite. The modeling results further revealed that the bulk rate of microbial Fe(II) oxidation in the system was controlled by the oxidation rate of Fe(II)-OXA complex, and the direct oxidation of structural Fe(II) by nitrate was negligible (Fig. 3f). A small amount of aqueous Fe^{2+} (0.6 mM) was measured within the first hour but became undetectable after that, suggesting that live cells quickly oxidized aqueous Fe^{2+} that may be released initially from rNAu-2. Interestingly, dissolved total Fe concentration was much higher than aqueous Fe^{2+} concentration (Fig. 4A), suggesting that Fe^{3+} from oxidation of aqueous Fe^{2+} remained soluble in the presence of OXA via complexation.

Again abiotic or heat-killed NTA groups did not exhibit any Fe(II) oxidation (Fig. 3g) or nitrate reduction (Fig. 3h). These controls showed similar concentrations of soluble Fe^{2+} and total Fe, suggesting that there was no soluble Fe^{3+} , and aqueous Fe^{2+} was derived from rNAu-2 possibly via chelation. However, unlike the OXA group, soluble Fe^{2+} showed a time-course increase (from 0.70 to 1.5 mM), likely due to continued dissolution of rNAu-2 by NTA. In the presence of live cells, Fe(II) in the NTA + cells group was rapidly oxidized in the first day followed by a slow oxidation afterwards (Figs. 3g & 3i) with the total extent of bio-oxidation reaching 85% (Table 1) after two spikes of nitrate addition. Microbes accounted for 93.1% of the total Fe(II) oxidation. Again the modeling results revealed that the bulk rate of microbial Fe(II) oxidation in the system was controlled by the oxidation rate of Fe(II)-NTA complex, and the direct oxidation of structural Fe(II) by nitrate was negligible (Fig. 3i). Similar to the OXA group, the concentration of total dissolved Fe was much higher than that of aqueous Fe^{2+} (Fig. 4B), suggesting that Fe^{3+} from oxidation of aqueous Fe^{2+} remained soluble via complexation with NTA. Interestingly, total dissolved Fe in biotic NTA group was much lower than those in abiotic and heat-killed controls (Fig. 4B), suggesting that live cells oxidized

rNAu-2 and thus may have stopped/slowed continuous dissolution of reduced NAu-2 by NTA.

Within the experimental period, no nitrite or ammonium was detected in all experimental groups, which is similar to previous observations (Weber et al., 2006b, Zhao et al., 2013, 2015, 2017; Chen et al., 2018, Liu et al., 2018). The majority of nitrate was reduced to N₂ at the end of day 16, with a small amount of N₂O observed in NTA and no-ligand group (Fig. 5). The total N₂ and N₂O produced in NTA, OXA, and the no ligand group (0.020 mmol, 0.015 mmol, 0.013 mmol, respectively) were close to half of the amount of nitrate reduction in the three biotic groups (0.0378 mmol, 0.032 mmol, 0.0379 mmol), which supports eq. 1 and previous observations (Chen et al., 2018; Liu et al., 2018).

3.1.2 Abiotic oxidation of rNAu-2 by nitrite

Although nitrite production was negligible, a supplementary experiment was performed to test Fe(II) oxidation by nitrite. The abiotic nitrite rNAu-2 oxidation supplementary experiment modeling results (Fig. 6) showed that the addition of OXA or NTA did not enhance significantly the rate of ferrous iron oxidation. The rate in rNAu-2, rNAu-2+OXA, and rNAu-2+NTA groups was 0.168 mM/d, 0.121 mM/d and 0.295 mM/d, respectively. According to the modeling results, the oxidation of OXA-Fe(II) and NTA-Fe(II) complex accounted for 5.4% and 40.6% of the total abiotic nitrite iron oxidation, respectively (Fig. 6c, f, and i). The bio-oxidation rate in the presence of NTA and OXA was about 7 times faster than the abiotic rate, while the no-ligand group was about one time faster than that. The pseudo-first order kinetic constant (Fig. 7) for biological Fe(II) oxidation in the presence of NTA and OXA and no-ligand group in the beginning of the experiment were 0.0497 h⁻¹ (R²=0.57), 0.0398 h⁻¹ (R²=0.74) and 0.0031 h⁻¹ (R²=0.99), respectively, while that for chemical Fe(II) oxidation by nitrite were 0.0028 h⁻¹ (R²=0.91), 0.0011 h⁻¹ (R²=0.83) and 0.0015 h⁻¹ (R²=0.90), respectively. A comparison between these constants revealed that biological oxidation of structural Fe(II) in rNAu-2 is much faster than chemical oxidation of Fe(II) by nitrite, with or without the presence of organic ligands. This is consistent with former observations in which nitrite oxidation contributed only a small fraction of Fe(II) oxidation while biological oxidation

plays a more important role in Fe oxidation in NDFO for Fe-bearing clay minerals (Shelobolina et al., 2012b; Zhao et al., 2013).

3.1.3. Spectroscopic evidence for Fe-OXA and Fe-NTA complex formation

To confirm complexation of Fe with OXA and NTA in these treatments, UV-vis absorption spectroscopy was performed. Characteristic peaks for Fe(III)-OXA complex at 260 nm (Pozdnyakov et al., 2008) and Fe(III)-NTA complex 258 nm (De et al., 2015), were observed for the OXA and NTA samples, respectively (Fig. 8). Unlike the biotic OXA group where the absorbance peak persisted until day 60 (Fig. 8C), the abiotic and heat-killed OXA control groups showed disappearance of the peak at day 16 (Figs. 8A, B), which is consistent with a time-course decrease of total Fe in these groups (Fig. 4A). In contrast, the absorbance peak for the abiotic and heat-killed NTA groups (Fig. 8D, E) showed a time-course increase, suggesting that aqueous Fe in these groups increased over time, consistent with measurements of aqueous Fe²⁺ and total Fe (Fig. 4B). The absorbance peak for the abiotic treatment did not show any time-course change, again consistent with nearly constant concentration of aqueous total Fe (Fig. 4B). The geochemical modeling using Visual Minteq 3.1 showed that Fe-oxalate and Fe-NTA⁻ were the dominant Fe-complexes in biotic OXA and NTA groups, respectively (Table 2), consistent with the UV-Vis spectroscopic results.

3.1.4 Interfacial electron transfer between Fe(III)-ligand complexes and rNAu-2

Co-existence of Fe(III)-ligand complexes (Figs. 3 & 8) and rNAu-2 suggests the possibility of interfacial electron transfer from structural Fe(II) of rNAu-2 to chelated Fe(III)-ligand complex. Therefore, a separate experiment was set up to directly test electron transfer from structural Fe(II) in rNAu-2 to Fe(III)-NTA. The first spike of Fe(III)-NTA (0.9 mM) was consumed instantaneously (Fig. 9A) and an equivalent amount of structural Fe(II) in rNAu-2 was oxidized (Fig. 9B). In the second spike, the redox reaction between Fe(II) in rNAu-2 and Fe(III)-NTA was instantaneous again, but only a half of the added Fe(III)-NTA (0.45 mM) was consumed and about 0.5 mM of structural Fe(II) oxidized. The third spike of Fe(III)-NTA (0.8 mM) showed that IET

almost stopped and structural Fe(II) remained at about 2.9 mM. The total oxidation extent was about 40% with three spikes of Fe(III)-NTA.

3.2 Effects of organic ligand on rNAu-2 dissolution

The observation of aqueous Fe^{2+} in the presence of OXA and NTA (Fig. 4) prompted us to explore the effects of these ligands on dissolution of rNAu-2. Aqueous concentrations of Si, Al, Fe, and Mg were measured throughout experimental period to monitor dissolution of rNAu-2. Aqueous Fe was negligible in the rNAu-2+Cell group without ligand (Fig. 10A). About 0.75 mM of aqueous total Fe was measured by day 2 in abiotic and heat-killed OXA controls, but aqueous Fe gradually decreased by day 60. In the presence of live cells, the level of aqueous Fe was maintained throughout the entire 60-day period, suggesting that cell activity oxidized Fe^{2+} to Fe^{3+} , which was maintained in the aqueous phase.

Fe concentrations were higher in abiotic NTA group than in abiotic OXA group increased over time (Fig. 10A), consistent with the trend of aqueous Fe^{2+} and total Fe over shorter time interval (Figs. 4A & B). However, in the presence of live cells and NTA, smaller amounts of Fe were measured in aqueous solution, suggesting that biotic oxidation of rNAu-2 may have inhibited dissolution of rNAu-2 by NTA.

Similar to Fe, low levels of aqueous Si were observed in the no-ligand group. Unlike the time-course decrease of Fe concentration in the abiotic and heat killed OXA groups (Figs. 4A & 10A), Si concentration first increased and then decreased (Fig. 10B) suggesting that Si precipitated later than Fe. In the two NTA abiotic groups, aqueous Si concentration increased over time, similar to Fe concentration (Fig. 10A). In the biotic NTA group aqueous Si concentration remained low until day 60, again similar to Fe

Aqueous Mg concentrations were low and similar across all OXA and NTA groups (Figure 10C). Similarly, aqueous Al concentrations were low, but showed a time-course decrease in most treatments (Figure 10D). The measured molar ratios of Fe/Si and Al/Si in aqueous solution varied over time, and were different from the corresponding molar ratios in the structural formula of rNAu-2, suggesting incongruent dissolution (Figure 11). In general, the Fe/Si ratios were higher than the corresponding ratio in rNAu-

2 (except for no ligand+cell group), and the Al/Si ratios were lower than the corresponding ratio in rNAu-2 (except those samples at day 2).

A comparison of aqueous Fe and Si concentration between the abiotic and biotic OXA/NTA groups showed lower dissolution of rNAu-2 in the presence of bacteria, suggesting that microbial oxidation of Fe(II) inhibited rNAu-2 dissolution. Indeed, the dissolution experiments of unreduced NAu-2 in the presence of OXA and NTA (Fig. 12) showed much lower levels of aqueous Fe, Si, Mg, and Al relative to those with rNAu-2 (Fig. 10). This finding confirmed that rNAu-2 was more susceptible to ligand-induced dissolution than oxidized NAu-2 (Kostka et al., 1999; Liu et al., 2018).

3.3 Mineralogical changes associated with nitrate-dependent Fe(II) oxidation

3.3.1 FTIR results

FTIR for the original NAu-2 showed an absorption band at 3554 cm^{-1} , which can be assigned to Fe-Fe-OH-stretching (Lee et al., 2006). Upon bio-reduction, this peak shifted to a lower wavelength of 3539 cm^{-1} with decreased intensity (Fig. 13). No peak shift or sharpening was observed in the abiotic OXA and NTA groups. However, upon bio-oxidation by Strain 2002, this peak shifted back to 3546 cm^{-1} for the no-ligand group and 3553 cm^{-1} for the organic ligand groups. In the absence of ligands, the broadened peak shape of rNAu-2 was not restored upon bio-oxidation, whereas in the presence of ligands, especially NTA, the peak shape was largely restored. Similar changes were observed for the absorption peak at 820 cm^{-1} , which can be attributed to Fe-Fe-OH bending (Gates et al., 2005). For example, bio-reduction of Fe(III) in NAu-2 shifted the peak from 818 cm^{-1} to 814 cm^{-1} and decreased its intensity, but bio-oxidation of Fe(II) in rNAu-2 sharpened the peak shape and shifted the position back to 816 cm^{-1} and 817 cm^{-1} , for the no-ligand group and the ligand-amended groups, respectively. These results indicated that bio-oxidation in the presence of organic ligands, especially NTA, better restored the NAu-2 structure.

3.3.2 XRD results

XRD patterns showed that nontronite was present as a dominant mineral in all the samples. Relative to un-reduced NAu-2, bio-reduction resulted in lower intensity and slightly broadened (001) peak (Fig. 14). The presence of OXA and NTA did not change the rNAu-2 peaks. In addition to nontronite, talc was detected in all groups after bio-reduction. After bio-oxidation for 60 days, the d(001) peak increased in intensity and became slightly sharper. In the OXA groups (with or without bacteria, reduced or oxidized NAu-2), whewellite, a hydrated calcium oxalate, with a formula $\text{CaC}_2\text{O}_4 \cdot \text{H}_2\text{O}$, was detected (Fig. 14). However, ferrosilite ($\text{Fe}_2\text{Si}_2\text{O}_6$) was only found in the abiotic rNAu-2 + OXA group (Fig. 15) and may be responsible for the time-course decrease aqueous concentrations of Fe and Si (Figs. 10A&B). Upon bio-oxidation, this ferrous mineral disappeared, likely because of a low level of aqueous Fe^{2+} (Fig. 4A). No new minerals were detected in the abiotic or biotic NTA group and no-ligand group.

3.3.3 SEM observations

SEM observations of the biotic NAu-2 groups showed cell association with rNAu-2 particles after 60 days (Fig. 16). No obvious cell encrustation was found in all biotic groups, even after 60 days of incubation (Fig. 16). This is consistent with our aqueous data showing low aqueous Fe in no-ligand group (Figs. 4 & 10) and solid-state oxidation of Fe(II) in rNAu-2 (Zhao et al., 2013, 2015). In the presence of ligands, Fe(III) should be in the soluble, complexed form (Figs. 4, 8, & 10), not in cell encrustation. The formation of whewellite in both abiotic and biotic OXA groups was confirmed by SEM observations (Fig. 17A). In the biotic and abiotic OXA groups, quartz was also observed, based on energy dispersive spectrum (EDS) (Fig. 17B), which would explain the decreased concentration of aqueous Si by day 60 (Fig. 10B). Ferrosilite was detected in the abiotic OXA group (Fig. 18C) but absent in biotic the group, consistent with XRD data (Fig. 14).

4. DISCUSSION

4.1 The effect of organic ligands on microbially catalyzed NDFO

Strain 2002 coupled oxidation of Fe(II) in rNAu-2 with reduction of nitrate to N₂ and N₂O (Fig. 5). The Fe(II) oxidation rate and extent were greatly enhanced by the presence of ligands. This effect is similar to that of organic matter on the reduction rate and extent of solid-phase Fe(III) by DIRB (Arnold et al., 1988; Lovley et al., 1996; Urrutia et al., 1998; Kostka et al., 1999; Urrutia et al., 1999; Royers et al., 2002a, b; Liu et al., 2017). Previous studies proposed that organic ligands can chelate with Fe(III) to form soluble Fe(III)-complexes and that organic matter can also function as electron shuttle to facilitate Fe(III) reduction (Urrutia et al., 1998; Kostka et al., 1999; Royers et al., 2002 a, b; Liu et al., 2017). However, similar mechanisms have not been proposed for the oxidation of structural Fe(II) in rNAu-2.

Without any ligands, Fe(II) oxidation occurred primarily in solid state (e.g., little aqueous concentrations of Fe²⁺ and total Fe, Fig. 4), consistent with previous studies (Zhao et al., 2013, 2015). In the presence of organic ligands (OXA and NTA), Fe(II) was partially liberated from the rNAu-2 structure (Fig. 4), leading to the formation of Fe(II)-oxalate and Fe(II)-NTA complexes (Fig. 8, Table 2). Because aqueous Fe²⁺ is oxidized much faster than structural Fe(II) in rNAu-2 in the NDFO process (Table 3) and in air (Zeng et al., 2019), the liberation of Fe(II) from solid to aqueous solution and formation of Fe(II)-OXA and Fe(II)-NTA complexes may have been responsible for the high rates of Fe(II) oxidation at the beginning of the experiment (Fig. 3d, g). This mechanism is similar to the one proposed for solid-form Fe(III) bio-reduction by DIRB in the presence of organic ligands (Lovley et al., 1996; Urrutia et al., 1999; Kostka et al., 1999; Royer et al., 2002).

However, the above Fe-complexation mechanism alone is not sufficient to fully explain the enhanced Fe(II) oxidation kinetics, because the amount of ligand-complexed Fe(II) was low (0.5 mM, Fig. 4) relative to a much higher amount of Fe(II) that's swiftly oxidized in the first day (~2.2 mM, Figs. 3d and g). Furthermore, it is unlikely that OXA and NTA initially dissolved a large fraction of rNAu-2 for subsequent oxidation, because the concentration of aqueous total Fe was maintained at a constant low level (e.g., 0.6mM, no time-course increase, Fig. 4). Therefore, an apparent paradox emerged

between the small amount of liberated aqueous Fe^{2+} and the much larger amount of Fe(II) oxidation observed in the first day for ligands amended groups. Thus, there should be a link that connects aqueous Fe(II)-complex oxidation and structural Fe(II) oxidation, as such this apparent paradox can be explained by invoking interfacial electron transfer (IET) from structural Fe(II) to oxidized ligand-complexed Fe(III) as a replenishing mechanism to sustain ligand-complexed Fe^{2+} . In this case, the overall oxidation rate was then dominated by the ligand-complexed aqueous Fe^{2+} , not by direct oxidation of structural Fe(II) before the bioavailable pool of structural Fe(II) for IET was exhausted. The supplementary experiment (Fig.9) and our previous observation for Fe(II)-NTA oxidation in air (Zeng et al., 2019) demonstrated the feasibility of this IET process. Previous studies have shown interfacial electron transfer from sorbed Fe(II) to structural Fe(III) in clay minerals (Schaefer et al., 2010; Neumann et al., 2013). Our data prompt us to propose a similar IET but in an opposite direction, e.g., from structural Fe(II) to aqueous, ligand-complexed Fe(III).

The above evidence collectively leads us to propose a model for ligand-facilitated Fe(II) oxidation in the biotic NDFO process (Fig. 18). Initially, organic ligands released some Fe(II) from rNAu-2 dissolution and formed Fe(II)-ligand complexes. Second, Fe(II)-ligand complexes were rapidly oxidized by strain 2002 through NDFO. Subsequently, aqueous Fe(III)-ligand complexes were re-reduced by structural Fe(II) in rNAu-2 via a reversed IET, leading to structural Fe(II) oxidation.

In addition to the enhancement of the Fe(II) oxidation rate, the presence of NTA and OXA also increased the oxidation extent of Fe(II) in rNAu-2 (85% and 83%, respectively) relative to the no-ligand control (about 48%). Our supplementary experiment showed that IET does not really enhance the oxidation extent, because repeated addition of Fe(III)-NTA only oxidized about 40% structural Fe(II) in rNAu-2 (Fig. 9). Therefore, other mechanisms may have increased the bio-available pool of Fe(II) when NTA and OXA were present. Possible reasons include ligand-promoted dissolution of rNAu-2 (Fig. 10) or breakup of rNAu-2 to smaller particles, both of which would make structural Fe(II) more available for bio-oxidation. Indeed, previous studies have observed that incongruent dissolution caused disintegration of clay particles to smaller

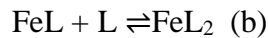
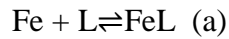
sizes (Ramos et al., 2011) and increased the surface area by organic ligands (Golubev et al., 2006) or inorganic acids (Komadel 2003; Carrado and Komadel 2009).

The non-stoichiometric ratio of oxidized Fe(II) to reduced nitrate was consistent with previous observations (Weber et al., 2009, Zhao et al., 2013, 2015, 2017; Chen et al., 2018, Liu et al., 2018). The modeling results suggest that the excess amount of nitrate consumption was due to heterotrophic nitrate reduction by stored carbon in 2002 cells or from nitrate assimilation. In addition, nitrate assimilation could also have contributed to extra nitrate consumption as well, because Strain 2002 is reported to be able to reproduce under both heterotrophic and lithoautotrophic conditions (Weber et al., 2006b). Nitrite was not accumulated in any groups, again consistent with previous studies (Weber et al., 2006b; Zhao et al., 2013; Chen et al., 2018; Liu et al., 2018). There could be two possible reasons: 1) in the NDFO process, nitrate was directly reduced to nitrogenous gases (N_2 and N_2O), or 2) nitrite was formed as a transient product that rapidly reacted with Fe(II) in NAu-2. Nonetheless, chemical Fe(II) oxidation by nitrite should be insignificant compared to biological oxidation (Figs. 6&7), consistent with previous observations in that nitrite, when present in small amounts, plays less important roles in Fe(II) oxidation compared to biological Fe(II) oxidation (Liu et al., 2018), and in that biological Fe(II) oxidation in clay minerals should be dominant in this process (Shelobolina et al., 2012b; Zhao et al., 2013).

4.2 Organic ligand effects on NAu-2 dissolution and secondary mineral precipitation

Our results suggest that OXA and NTA, as strong metal chelators, can enhance dissolution of bio-reduced NAu-2 (Figs. 4&10). Reduced smectite is less stable than unreduced smectite probably due to reduction-induced dehydroxylation (Stucki et al., 1996, Manceau et al., 2000), and can therefore readily dissolve in the presence of ligands (Kostka et al., 1999). The dissolved Fe/Si and Al/Si molar ratios were not in line with that in the NAu-2 ($M_{0.72}(Si_{7.55}Al_{0.45})(Fe_{3.83}Mg_{0.05})O_{20}(OH)_4$) structure in both the OXA and NTA groups (Fig. 11), suggesting incongruent dissolution. However, the ATR-FTIR spectra for the post-dissolution residual rNAu-2 were similar to those for the original rNAu-2, suggesting that OXA and NTA only dissolved some rNAu-2, possibly small and poorly crystalline rNAu-2, but did not alter the structure of the residual rNAu-2. This

effect of OXA and NTA is in contrast to a previous observation where the presence of humic acid drastically changed the smectite structure (Liu et al., 2017). This difference is probably because nontronite is less susceptible to dissolution by OXA and NTA than by humic acid. Between the two ligands, NTA promoted more extensive dissolution of rNAu-2 than OXA. When OXA and NTA were added to rNAu-2, they would form Fe(II)-ligand complexes through the following steps, where L represents different ligands (Tada et al., 2011):



The log stability constants of Fe(II) with oxalate in (a) and (b) were 3.05 and 5.15, respectively, while those for NTA were 8.83 and 12.8, respectively (Micskei. et al., 1987). Therefore, when Fe was chelated by NTA, the strong chelating ability of NTA prevented Fe(II) from precipitating, while Fe in the OXA abiotic groups was more likely to precipitate as ferrosilite ($\text{Fe}_2\text{Si}_2\text{O}_6$) (Fig. 15, 17C).

Unexpectedly, the presence of live 2002 cells resulted in less dissolution relative to the abiotic groups (Figs. 4A&B, 10A&B), suggesting that microbial oxidation of rNAu-2 back to NAu-2 stabilized the NAu-2 structure. Indeed, unreduced NAu-2 showed a lower amount of ligand-induced dissolution than rNAu-2 (Fig. 12). Bio-oxidation of Fe^{2+} to Fe^{3+} also prevented precipitation of ferrosilite in the OXA group, because of a negligible level of aqueous Fe^{2+} (Fig. 4A). Bio-oxidation not only stabilized the NAu-2 structure against dissolution, but also restored the bioreduction-induced, altered structure back to its original integrity, as evidenced by restoration of the d(001) peak sharpness (Fig. 14) and both Fe-Fe-OH stretching and bending peaks in FTIR spectra (Fig. 13). The restoration was more complete in the presence of OXA and NTA, apparently because of the higher extents of structural Fe(II) oxidation in the ligand treatment groups (Figs. 3d&g).

4.3 Environmental implication

Although previous studies have unraveled chemically and microbially mediated Fe-redox cycling in clay minerals (Lee et al., 2006; Shelobolina et al., 2012b; Dong 2012; Zhao et al., 2013, 2015,2017), the effects of organic matter on the Fe-redox cycle have

remained understudied. Our findings expand previous understandings of the microbially-mediated Fe-redox cycle by including the role of organic ligands in mediating the process.. The results of this study demonstrated that the rate and extent of Fe(II) oxidation in rNAu-2 by nitrate-dependent iron oxidizers were strongly enhanced by the presence of organic ligands, similar to their role in Fe(III) reduction process. Thus, in various natural environments like soils, aquatic systems and sediments, where organic matter and clay minerals are abundant (Lovley et al., 1986; Kahle et al., 2004; Lehmann et al., 2015), organic ligands are expected to play significant roles in Fe redox cycles of clay minerals. More important, this study suggests that ligand-complexed, aqueous Fe^{2+} and Fe^{3+} can function as effective “electron shuttles” to increase the bioavailability of solid-state Fe, which may not be otherwise redox available or active. This would have major implications for several environmental processes, because clays minerals are ubiquitous and they play very important roles in nutrient cycling and contaminant transformation (Dong 2012). Thus, organic ligands are expected to affect the fate and transport of nutrients and contaminants in the environment. The role of organic matter should be further studied to better understand the coupled Fe, C, and N cycles in nature, and to maximize the benefits in environmental remediation process.

Apart from their influence on Fe redox process, organic ligands can also induce mineral dissolution-precipitation, thus altering the petrophysical property of soils and sediments. At DOE contamination sites like Hanford, where dumped wastes contain NTA as high as 5.2 -10.5 mM (Bucheli-Witschel et al., 2001), the physicochemical properties of soils and sediments could have been impacted through mineral dissolution-and re-precipitation, which further affects contaminant transport. Furthermore, clay minerals, due to their low permeability, have previously been proposed as landfill and nuclear waste disposal barrier materials (Wong et al., 2017; Claret et al., 2018). However, dissolution and secondary mineral formation induced by organic matter may alter the porosity and permeability of clay minerals, and thus alter their utility as backfill materials. For example, Schindler and Singer (2017) proposed that mineral surface coatings formed from dissolution-reprecipitation contain complex and variable porosities that affect solute diffusion and transport. Therefore, such organic matter effects on the physicochemical properties of clay minerals should be investigated further to better

understand contaminant transport and potential application of clay for contaminant disposal.

5. CONCLUSIONS

Oxalate and NTA enhanced the rate and extent of microbially-mediated oxidation of structural Fe(II) in reduced nontronite by *Pseudogulbenkiania* sp. strain 2002. A much higher rate of bio-oxidation of structural Fe(II) in rNAu-2 than the Fe(II) oxidation rate by nitrite in NAu-2 suggests a dominating biological role in the NDFO process. Dissolution of structural Fe(II) and formation of soluble Fe(II)-ligand complexes accounted for its rapid rate of Fe(II) oxidation because aqueous Fe²⁺ is oxidized more rapidly than structural Fe(II). The rapid rate of Fe(II) oxidation is maintained through interfacial electron transfer from structural Fe(II) in rNAu-2 to Fe(III)-ligand complexes. Ligand-promoted dissolution and particle fragmentation are responsible for enhanced extent of Fe(II) oxidation. The presence of oxalate and NTA enhanced incongruent dissolution of rNAu-2. Dissolved Fe and Si in abiotic oxalate groups were precipitated with quartz and ferrosilite formation while dissolved Fe and Si were not precipitated in abiotic or biotic NTA groups due to its strong chelating ability. The results of this study highlight the influence of organic ligands on microbially mediated Fe oxidation kinetics, mineral dissolution-precipitation, and mineral transformations.

REFERENCES

- Amonette, J. E., and Templeton, J. C. (1998). Improvements to the quantitative assay of nonrefractory minerals for Fe (II) and total Fe using 1, 10-phenanthroline. *Clays and Clay Minerals*, **46**, 51-62.
- Arnold, R. G., DiChristina, T. J., and Hoffmann, M. R. (1988). Reductive dissolution of Fe (III) oxides by *Pseudomonas* sp. 200. *Biotechnology and Bioengineering*, **32**, 1081-1096.
- Bethke, C.M. (2008) *Geochemical and Biogeochemical Reaction Modeling*, 2nd ed. Cambridge University Press, Cambridge, UK.
- Bishop, M. E., Glasser, P., Dong, H., Arey, B., and Kovarik, L. (2014). Reduction and immobilization of hexavalent chromium by microbially reduced Fe-bearing clay minerals. *Geochimica et Cosmochimica Acta*, **133**, 186-203.
- Bott, T. (1980). *The effect of nitrilotriacetic acid (NTA) on the structure and functioning of aquatic communities in streams*. Environmental Research Laboratory, Office of Research and Development, US Environmental Protection Agency.
- Braissant, O., Cailleau, G., Aragno, M., and Verrecchia, E. P. (2004). Biologically induced mineralization in the tree *Milicia excelsa* (Moraceae): its causes and consequences to the environment. *Geobiology*, **2**, 59-66.
- Bryce, C., Blackwell, N., Schmidt, C., Otte, J., Huang, Y. M., Kleindienst, S., and Byrne, J. M. (2018). Microbial anaerobic Fe (II) oxidation—Ecology, mechanisms and environmental implications. *Environmental microbiology*, **20**, 3462-3483.
- Bucheli-Witschel, M., and Egli, T. (2001). Environmental fate and microbial degradation of aminopolycarboxylic acids. *FEMS microbiology reviews*, **25**, 69-106.
- Burford, E. P., Hillier, S., and Gadd, G. M. (2006). Biomineralization of fungal hyphae with calcite (CaCO₃) and calcium oxalate mono- and dihydrate in carboniferous limestone microcosms. *Geomicrobiology Journal*, **23**, 599-611.
- Burton, E. D., Hockmann, K., Karimian, N., and Johnston, S. G. (2019). Antimony mobility in reducing environments: The effect of microbial iron (III)-reduction and associated secondary mineralization. *Geochimica et Cosmochimica Acta*, **245**, 278-289.

- Byrne-Bailey, K. G., Weber, K. A., Bose, S., Knox, T., Spanbauer, T. L., Chertkov, O., and Coates, J. D. (2010). Completed genome sequence of the anaerobic iron-oxidizing bacterium *Acidovorax ebreus* strain TPSY. *Journal of bacteriology*, **192**, 1475-1476.
- Carlson, H. K., Clark, I. C., Blazewicz, S. J., Iavarone, A. T., and Coates, J. D. (2013). Fe (II) oxidation is an innate capability of nitrate-reducing bacteria that involves abiotic and biotic reactions. *Journal of bacteriology*, **195**, 3260-3268.
- Carrado, K. A., and Komadel, P. (2009). Acid activation of bentonites and polymer-clay nanocomposites. *Elements*, **5**, 111-116.
- Chakraborty, A., Roden, E. E., Schieber, J., & Picardal, F. (2011). Enhanced growth of *Acidovorax* sp. strain 2AN during nitrate-dependent Fe (II) oxidation in batch and continuous-flow systems. *Appl. Environ. Microbiol.*, **77**, 8548-8556.
- Chakraborty, A., & Picardal, F. (2013). Neutrophilic, nitrate-dependent, Fe (II) oxidation by a *Dechloromonas* species. *World Journal of Microbiology and Biotechnology*, **29**, 617-623.
- Claret, F., Marty, N., and Tournassat, C. (2018). Modeling the Long-term Stability of Multi-barrier Systems for Nuclear Waste Disposal in Geological Clay Formations. *Reactive Transport Modeling: Applications in Subsurface Energy and Environmental Problems*, 395-451.
- De Luca, A., Dantas, R. F., and Esplugas, S. (2015). Study of Fe (III)-NTA chelates stability for applicability in photo-Fenton at neutral pH. *Applied Catalysis B: Environmental*, **179**, 372-379.
- Dong, H., Kukkadapu, R. K., Fredrickson, J. K., Zachara, J. M., Kennedy, D. W., & Kostandarithes, H. M. (2003). Microbial reduction of structural Fe (III) in illite and goethite. *Environmental Science & Technology*, **37**, 1268-1276.
- Dong, H., Jaisi, D. P., Kim, J., and Zhang, G. (2009). Microbe-clay mineral interactions. *American Mineralogist*, **94**, 1505-1519.
- Dong, H. (2012). Clay–microbe interactions and implications for environmental mitigation. *Elements*, **8**, 113-118.
- Emerson, D., Fleming, E. J., and McBeth, J. M. (2010). Iron-oxidizing bacteria: an environmental and genomic perspective. *Annual review of microbiology*, **64**, 561-583.

- Ernstsen, V. (1996). Reduction of nitrate by Fe 2+ in clay minerals. *Clays and Clay Minerals*, **44**, 599-608.
- Ernstsen, V., Gates, W. P., and Stucki, J. W. (1998). Microbial reduction of structural iron in clays—a renewable source of reduction capacity. *Journal of Environmental Quality*, **27**, 761-766.
- Fialips, C. I., Huo, D., Yan, L., Wu, J., and Stucki, J. W. (2002). Infrared study of reduced and reduced-reoxidized ferruginous smectite. *Clays and Clay minerals*, **50**, 455-469.
- Fox, T. R., and Comerford, N. B. (1990). Low-molecular-weight organic acids in selected forest soils of the southeastern USA. *Soil Science Society of America Journal*, **54**, 1139-1144.
- Frost, R. L., Klopogge, J. T., and Ding, Z. (2002). The Garfield and Uley nontronites—An infrared spectroscopic comparison. *Spectrochimica Acta Part A: Molecular and Biomolecular Spectroscopy*, **58**, 1881-1894.
- Fujii, M., Imaoka, A., Yoshimura, C., and Waite, T. D. (2014). Effects of molecular composition of natural organic matter on ferric iron complexation at circumneutral pH. *Environmental science and technology*, **48**, 4414-4424.
- Gates, W. P., Slade, P. G., Manceau, A., and Lanson, B. (2002). Site occupancies by iron in nontronites. *Clays and Clay Minerals*, **50**, 223-239.
- Gates, W. (2005). Infrared spectroscopy and the chemistry of dioctahedral smectites. *The Application of Vibrational Spectroscopy to Clay Minerals and Layered Double Hydroxides*, 126-168.
- Golubev, S. V., Bauer, A., and Pokrovsky, O. S. (2006). Effect of pH and organic ligands on the kinetics of smectite dissolution at 25 C. *Geochimica et Cosmochimica Acta*, **70**, 4436-4451.
- Gröhlich, A., Langer, M., Mitrakas, M., Zouboulis, A., Katsoyiannis, I., and Ernst, M. (2017). Effect of organic matter on Cr (VI) removal from groundwaters by Fe (II) reductive precipitation for groundwater treatment. *Water*, **9**, 389.
- He, Q. X., Huang, X. C., and Chen, Z. L. (2011). Influence of organic acids, complexing agents and heavy metals on the bioleaching of iron from kaolin using Fe (III)-reducing bacteria. *Applied Clay Science*, **51**, 478-483.

- He, S., Tominski, C., Kappler, A., Behrens, S., and Roden, E. E. (2016). Metagenomic analyses of the autotrophic Fe (II)-oxidizing, nitrate-reducing enrichment culture KS. *Appl. Environ. Microbiol.*, **82**, 2656-2668.
- Hedrich, S., Schlömann, M., and Johnson, D. B. (2011). The iron-oxidizing proteobacteria. *Microbiology*, **157**, 1551-1564.
- Hopwood, M. J., Statham, P. J., Skrabal, S. A., and Willey, J. D. (2015). Dissolved iron (II) ligands in river and estuarine water. *Marine Chemistry*, **173**, 173-182.
- Instruments, L. (2003). Determination of nitrate/nitrite in surface and wastewaters by flow injection analysis. *QuickChem Method*, 10-107.
- Ito, A., and Wagai, R. (2017). Global distribution of clay-size minerals on land surface for biogeochemical and climatological studies. *Scientific data*, **4**, 170103.
- Jaisi, D. P., Kukkadapu, R. K., Eberl, D. D., and Dong, H. (2005). Control of Fe (III) site occupancy on the rate and extent of microbial reduction of Fe (III) in nontronite. *Geochimica et Cosmochimica Acta*, **69**, 5429-5440.
- Jaisi, D. P., Dong, H., and Liu, C. (2007). Influence of biogenic Fe (II) on the extent of microbial reduction of Fe (III) in clay minerals nontronite, illite, and chlorite. *Geochimica et Cosmochimica Acta*, **71**, 1145-1158.
- Jaisi, D. P., Dong, H., and Morton, J. P. (2008). Partitioning of Fe (II) in reduced nontronite (NAu-2) to reactive sites: Reactivity in terms of Tc (VII) reduction. *Clays and Clay Minerals*, **56**, 175-189.
- Jamieson, J., Prommer, H., Kaksonen, A. H., Sun, J., Siade, A. J., Yusov, A., and Bostick, B. (2018). Identifying and quantifying the intermediate processes during nitrate-dependent iron (II) oxidation. *Environmental science and technology*, **52**, 5771-5781.
- Jansen, B., Nierop, K. G., and Verstraten, J. M. (2003). Mobility of Fe (II), Fe (III) and Al in acidic forest soils mediated by dissolved organic matter: influence of solution pH and metal/organic carbon ratios. *Geoderma*, **113**, 323-340.
- Jin, Q., and Roden, E. E. (2011). Microbial physiology-based model of ethanol metabolism in subsurface sediments. *Journal of contaminant hydrology*, **125**, 1-12.
- Jones, D. L. (1998). Organic acids in the rhizosphere—a critical review. *Plant and soil*, **205**, 25-44.

- Kahle, M., Kleber, M., and Jahn, R. (2004). Retention of dissolved organic matter by phyllosilicate and soil clay fractions in relation to mineral properties. *Organic Geochemistry*, **35**, 269-276.
- Kappler, A., and Newman, D. K. (2004). Formation of Fe (III)-minerals by Fe (II)-oxidizing photoautotrophic bacteria. *Geochimica et Cosmochimica Acta*, **68**, 1217-1226.
- Kappler, A., Schink, B., and Newman, D. K. (2005a). Fe (III) mineral formation and cell encrustation by the nitrate-dependent Fe (II)-oxidizer strain BoFeN1. *Geobiology*, **3**, 235-245.
- Kappler, A., and Straub, K. L. (2005b). Geomicrobiological cycling of iron. *Reviews in Mineralogy and Geochemistry*, **59**, 85-108.
- Keeling, J. L., Raven, M. D., and Gates, W. P. (2000). Geology and characterization of two hydrothermal nontronites from weathered metamorphic rocks at the Uley graphite mine, South Australia. *Clays and Clay Minerals*, **48**, 537-548.
- Kim, J., Dong, H., Seabaugh, J., Newell, S. W., and Eberl, D. D. (2004). Role of microbes in the smectite-to-illite reaction. *Science*, **303**, 830-832.
- Kiskira, K., Papirio, S., van Hullebusch, E. D., and Esposito, G. (2017). Influence of pH, EDTA/Fe (II) ratio, and microbial culture on Fe (II)-mediated autotrophic denitrification. *Environmental Science and Pollution Research*, **24**, 21323-21333.
- Klueglein, N., Zeitvogel, F., Stierhof, Y. D., Floetenmeyer, M., Konhauser, K. O., Kappler, A., & Obst, M. (2014). Potential role of nitrite for abiotic Fe (II) oxidation and cell encrustation during nitrate reduction by denitrifying bacteria. *Appl. Environ. Microbiol.*, **80**, 1051-1061.
- Klueglein, N., Picardal, F., Zedda, M., Zwiener, C., and Kappler, A. (2015). Oxidation of Fe(II)-EDTA by nitrite and by two nitrate-reducing Fe (II)-oxidizing Acidovorax strains. *Geobiology*, **13**, 198-207.
- Komadell, P. (2016). Chemically modified smectites. *Clay Minerals*, **38**, pp. 127-138.
- Kostka, J. E., Stucki, J. W., Nealson, K. H., and Wu, J. (1996). Reduction of structural Fe (III) in smectite by a pure culture of *Shewanella putrefaciens* strain MR-1. *Clays and Clay Minerals*, **44**, 522-529.

- Kostka, J. E., Haefele, E., Viehweger, R., and Stucki, J. W. (1999). Respiration and dissolution of iron (III)-containing clay minerals by bacteria. *Environmental Science and Technology*, **33**, 3127-3133.
- Laufer, K., Nordhoff, M., Halama, M., Martinez, R. E., Obst, M., Nowak, M., ... and Kappler, A. (2017). Microaerophilic Fe (II)-oxidizing Zetaproteobacteria isolated from low-Fe marine coastal sediments: physiology and composition of their twisted stalks. *Appl. Environ. Microbiol.*, **83**, e03118-16.
- Lee, K., Kostka, J. E., and Stucki, J. W. (2006). Comparisons of structural Fe reduction in smectites by bacteria and dithionite: An infrared spectroscopic study. *Clays and Clay Minerals*, **54**, 195-208.
- Lehmann, J., and Kleber, M. (2015). The contentious nature of soil organic matter. *Nature*, **528**, 60.
- Li, X., Zhang, W., Liu, T., Chen, L., Chen, P., and Li, F. (2016). Changes in the composition and diversity of microbial communities during anaerobic nitrate reduction and Fe (II) oxidation at circumneutral pH in paddy soil. *Soil Biology and Biochemistry*, **94**, 70-79.
- Lin, C., Larsen, E. I., Nothdurft, L. D., and Smith, J. J. (2012). Neutrophilic, microaerophilic Fe (II)-oxidizing bacteria are ubiquitous in aquatic habitats of a subtropical Australian coastal catchment (ubiquitous FeOB in catchment aquatic habitats). *Geomicrobiology Journal*, **29**, 76-87.
- Liu, D., Dong, H., Bishop, M. E., Wang, H., Agrawal, A., Tritschler, S., ... and Xie, S. (2011). Reduction of structural Fe (III) in nontronite by methanogen *Methanosarcina barkeri*. *Geochimica et Cosmochimica Acta*, **75**, 1057-1071.
- Liu, G., Qiu, S., Liu, B., Pu, Y., Gao, Z., Wang, J., ... and Zhou, J. (2017). Microbial reduction of Fe (III)-bearing clay minerals in the presence of humic acids. *Scientific reports*, **7**, 45354.
- Liu, T., Chen, D., Luo, X., Li, X., and Li, F. (2018). Microbially mediated nitrate-reducing Fe (II) oxidation: Quantification of chemodenitrification and biological reactions. *Geochimica et Cosmochimica Acta*.

- Liu, X., Dong, H., Yang, X., Kovarik, L., Chen, Y., and Zeng, Q. (2018). Effects of citrate on hexavalent chromium reduction by structural Fe (II) in nontronite. *Journal of hazardous materials*, **343**, 245-254.
- Lovley, D. R., and Phillips, E. J. (1986). Organic matter mineralization with reduction of ferric iron in anaerobic sediments. *Appl. Environ. Microbiol.*, **51**, 683-689.
- Lovley, D. R., Woodward, J. C., and Chapelle, F. H. (1994). Stimulated anoxic biodegradation of aromatic hydrocarbons using Fe (III) ligands. *Nature*, **370**, 128.
- Lovley, D. R., and Woodward, J. C. (1996). Mechanisms for chelator stimulation of microbial Fe (III)-oxide reduction. *Chemical Geology*, **132**, 19-24.
- Luther III, G. W., Kostka, J. E., Church, T. M., Sulzberger, B., and Stumm, W. (1992). Seasonal iron cycling in the salt-marsh sedimentary environment: the importance of ligand complexes with Fe (II) and Fe (III) in the dissolution of Fe (III) minerals and pyrite, respectively. *Marine chemistry*, **40**, 81-103.
- Luther III, G. W., Shellenbarger, P. A., and Brendel, P. J. (1996). Dissolved organic Fe (III) and Fe (II) complexes in salt marsh porewaters. *Geochimica et Cosmochimica Acta*, **60**, 951-960.
- Manceau, A., Lanson, B., Drits, V. A., Chateigner, D., Gates, W. P., Wu, J., ... and Stucki, J. W. (2000). Oxidation-reduction mechanism of iron in dioctahedral smectites: I. Crystal chemistry of oxidized reference nontronites. *American Mineralogist*, **85**, 133-152.
- Melton, E. D., Swanner, E. D., Behrens, S., Schmidt, C., and Kappler, A. (2014). The interplay of microbially mediated and abiotic reactions in the biogeochemical Fe cycle. *Nature Reviews Microbiology*, **12**, 797.
- Micskei, K. (1987). Equilibria in aqueous solutions of some iron (II) complexes. *Journal of the Chemical Society, Dalton Transactions*, **1**, 255-257.
- Moore, D. M., & Reynolds, R. C. (1989). *X-ray Diffraction and the Identification and Analysis of Clay Minerals* (Vol. 322, p. 321). Oxford: Oxford university press.
- Neilands, J. B. (1981). Microbial iron compounds. *Annual review of biochemistry*, **50**(1), 715-731.

- Neumann, A., Olson, T. L., and Scherer, M. M. (2013). Spectroscopic evidence for Fe (II)–Fe (III) electron transfer at clay mineral edge and basal sites. *Environmental science and technology*, **47**, 6969-6977.
- Pantke, C., Obst, M., Benzerara, K., Morin, G., Ona-Nguema, G., Dippon, U., & Kappler, A. (2012). Green rust formation during Fe (II) oxidation by the nitrate-reducing *Acidovorax* sp. strain BoFeN1. *Environmental science & technology*, **46**, 1439-1446.
- Parrello, D., Zegeye, A., Mustin, C., and Billard, P. (2016). Siderophore-mediated iron dissolution from nontronites is controlled by mineral cristallochemistry. *Frontiers in microbiology*, **7**, 423.
- Peng, C., Sundman, A., Bryce, C., Catrouillet, C., Borch, T., & Kappler, A. (2018). Oxidation of Fe (II)–Organic Matter Complexes in the Presence of the Mixotrophic Nitrate-Reducing Fe (II)-Oxidizing Bacterium *Acidovorax* sp. BoFeN1. *Environmental science & technology*, **52**, 5753-5763.
- Perdue, E. M., BECK, K. C., and Reuter, J. H. (1976). Organic complexes of iron and aluminium in natural waters. *Nature*, **260**, 418.
- Petschick, R., Kuhn, G., and Gingele, F. (1996). Clay mineral distribution in surface sediments of the South Atlantic: sources, transport, and relation to oceanography. *Marine Geology*, **130**, 203-229.
- Picardal, F. (2012). Abiotic and microbial interactions during anaerobic transformations of Fe (II) and NO_x. *Frontiers in microbiology*, **3**, 112.
- Pozdnyakov, I. P., Kel, O. V., Plyusnin, V. F., Grivin, V. P., and Bazhin, N. M. (2008). New insight into photochemistry of ferrioxalate. *The Journal of Physical Chemistry A*, **112**, 8316-8322.
- Ramos, M. E., Cappelli, C., Rozalén, M., Fiore, S., and Huertas, F. J. (2011). Effect of lactate, glycine, and citrate on the kinetics of montmorillonite dissolution. *American Mineralogist*, **96**, 768-780.
- Vindedahl, A. M., Strehlau, J. H., Arnold, W. A., and Penn, R. L. (2016). Organic matter and iron oxide nanoparticles: aggregation, interactions, and reactivity. *Environmental Science: Nano*, **3**, 494-505.
- Rose, A. L., and Waite, T. D. (2003). Kinetics of iron complexation by dissolved natural organic matter in coastal waters. *Marine chemistry*, **84**, 85-103.

- Royer, R. A., Burgos, W. D., Fisher, A. S., Unz, R. F., & Dempsey, B. A. (2002a). Enhancement of biological reduction of hematite by electron shuttling and Fe (II) complexation. *Environmental science & technology*, **36**, 1939-1946.
- Royer, R. A., Burgos, W. D., Fisher, A. S., Jeon, B. H., Unz, R. F., & Dempsey, B. A. (2002b). Enhancement of hematite bioreduction by natural organic matter. *Environmental science & technology*, **36**, 2897-2904.
- Schaefer, M. V., Gorski, C. A., and Scherer, M. M. (2010). Spectroscopic evidence for interfacial Fe (II)– Fe (III) electron transfer in a clay mineral. *Environmental Science and Technology*, **45**, 540-545.
- Schaedler, F., Kappler, A., and Schmidt, C. (2018). A revised iron extraction protocol for environmental samples rich in nitrite and carbonate. *Geomicrobiology Journal*, **35**, 23-30.
- Schindler, M., and Singer, D. M. (2017). Mineral surface coatings: Environmental records at the Nanoscale. *Elements: An International Magazine of Mineralogy, Geochemistry, and Petrology*, **13**, 159-164.
- Scholz, F., Löscher, C. R., Fiskal, A., Sommer, S., Hensen, C., Lomnitz, U., ... and Canfield, D. E. (2016). Nitrate-dependent iron oxidation limits iron transport in anoxic ocean regions. *Earth and Planetary Science Letters*, **454**, 272-281.
- Sharma, P., Ofner, J., and Kappler, A. (2010). Formation of binary and ternary colloids and dissolved complexes of organic matter, Fe and As. *Environmental science and technology*, **44**, 4479-4485.
- Shelobolina, E., Xu, H., Konishi, H., Kukkadapu, R., Wu, T., Blöthe, M., & Roden, E. (2012a). Microbial lithotrophic oxidation of structural Fe (II) in biotite. *Appl. Environ. Microbiol.*, **78**, 5746-5752.
- Shelobolina, E. S., Konishi, H., Xu, H., Benzine, J., Xiong, M. Y., Wu, T., ... and Roden, E. (2012b). Isolation of phyllosilicate–iron redox cycling microorganisms from an illite–smectite rich hydromorphic soil. *Frontiers in Microbiology*, **3**, 134.
- Stern, N., Mejia, J., He, S., Yang, Y., Ginder-Vogel, M., and Roden, E. E. (2018). Dual role of humic substances as electron donor and shuttle for dissimilatory iron reduction. *Environmental science and technology*, **52**, 5691-5699.

- Straub, K. L., Benz, M., Schink, B., and Widdel, F. (1996). Anaerobic, nitrate-dependent microbial oxidation of ferrous iron. *Appl. Environ. Microbiol.*, **62**, 1458-1460.
- Stucki, J. W., Bailey, G. W., and Gan, H. (1996). Oxidation-reduction mechanisms in iron-bearing phyllosilicates. *Applied Clay Science*, **10**, 417-430.
- Stucki, J. W., & Kostka, J. E. (2006). Microbial reduction of iron in smectite. *Comptes Rendus Geoscience*, **338**, 468-475.
- Tada, R. M. (2011). *Synthesis and characterization of some transition metal complexes* (Doctoral dissertation, Saurashtra University).
- Taillefert, M., Bono, A. B., and Luther, G. W. (2000). Reactivity of freshly formed Fe (III) in synthetic solutions and (pore) waters: voltammetric evidence of an aging process. *Environmental science and technology*, **34**, 2169-2177.
- Urrutia, M. M., Roden, E. E., & Zachara, J. M. (1999). Influence of aqueous and solid-phase Fe (II) complexants on microbial reduction of crystalline iron (III) oxides. *Environmental Science & Technology*, **33**, 4022-4028.
- Weber, K. A., Picardal, F. W., and Roden, E. E. (2001). Microbially catalyzed nitrate-dependent oxidation of biogenic solid-phase Fe (II) compounds. *Environmental Science and Technology*, **35**, 1644-1650.
- Weber, K. A., Achenbach, L. A., and Coates, J. D. (2006a). Microorganisms pumping iron: anaerobic microbial iron oxidation and reduction. *Nature Reviews Microbiology*, **4**, 752.
- Weber, K. A., Pollock, J., Cole, K. A., O'Connor, S. M., Achenbach, L. A., and Coates, J. D. (2006b). Anaerobic nitrate-dependent iron (II) bio-oxidation by a novel lithoautotrophic betaproteobacterium, strain 2002. *Appl. Environ. Microbiol.*, **72**, 686-694.
- Weber, K. A., Hedrick, D. B., Peacock, A. D., Thrash, J. C., White, D. C., Achenbach, L. A., and Coates, J. D. (2009). Physiological and taxonomic description of the novel autotrophic, metal oxidizing bacterium, *Pseudogulbenkiania* sp. strain 2002. *Applied Microbiology and Biotechnology*, **83**(3), 555-565.
- Wong, J. T. F., Chen, Z., Chen, X., Ng, C. W. W., and Wong, M. H. (2017). Soil-water retention behavior of compacted biochar-amended clay: a novel landfill final cover material. *Journal of soils and sediments*, **17**, 590-598.

- Xiong, M. Y., Shelobolina, E. S., and Roden, E. E. (2015). Potential for microbial oxidation of ferrous iron in basaltic glass. *Astrobiology*, **15**, 331-340.
- Zeng, Q., Dong, H., and Wang, X. (2019). Effect of ligands on the production of oxidants from oxygenation of reduced Fe-bearing clay mineral nontronite. *Geochimica et Cosmochimica Acta*, **251**, 136-156.
- Zhang, G., Senko, J. M., Kelly, S. D., Tan, H., Kemner, K. M., and Burgos, W. D. (2009). Microbial reduction of iron (III)-rich nontronite and uranium (VI). *Geochimica et Cosmochimica Acta*, **73**, 3523-3538.
- Zhou, J., Wang, H., Yang, K., Ji, B., Chen, D., Zhang, H., ... and Tian, J. (2016). Autotrophic denitrification by nitrate-dependent Fe (II) oxidation in a continuous up-flow biofilter. *Bioprocess and biosystems engineering*, **39**, 277-284.

TABLE CAPTIONS

Table 1. Fe(II) concentration before and after bio-oxidation, and bio-oxidation extent and rate in different cell treatment groups.

Table 2. Calculated Fe(II) speciation (Visual MINTEQ 3.1) of cell treatment groups in the presence of NTA or OXA.

Table 3. Aqueous Fe²⁺ or clay structural Fe(II) oxidation rate by Strain 2002 in NDFO. Bio-oxidation of aqueous Fe²⁺ is faster than of structural Fe(II) in rNAu-2.

FIGURE CAPTIONS

Figure 1. A: Strain 2002 growth curve after one-round aqueous medium culture activation from frozen stock; B: Cell number correlation with OD 600nm absorbance ($R^2=0.9984$).

Figure 2. Growth curve of Strain 2002 on acetate, oxalate and NTA. Duplicate cultures are shown in solid and dash lines, respectively. No growth was observed in the presence of nitrilotriacetic acid (NTA) and oxalate (OXA) as sole carbon substrate. Duplicate cultures are shown in solid and dash lines, respectively.

Figure 3. Time-course concentration change of: total Fe(II) (dissolved in solution + structural Fe(II) in rNAu-2), nitrate, and nitrite in NDFO without the addition of ligand (a-c), and in the presence of OXA (d-f) and NTA (g-i). Data points are experimental results (\circ , with cells; \square , no cells abiotic; \times , heat-killed control), and error bars are the standard deviation of replicate experiments; solid lines are the modeling results. Jump of nitrate concentration at day 16 stands for a second spike of nitrate. Abiotic controls in the no-ligand group were not considered as Zhao et al. (2013, 2015, 2017) had observed no reaction in such groups. No nitrate reduction or Fe(II) oxidation were observed in no cells abiotic or heat-killed control group for OXA and NTA groups. The presence of OXA (d) and NTA (g) enhanced Fe(II) oxidation rate and extent than no ligand group (a).

Figure 4. Time-course change of dissolved aqueous Fe^{2+} and total aqueous Fe in NDFO. A: OXA groups. B: NTA groups. Negligible amounts of soluble Fe^{2+} and total aqueous Fe were measured in no ligand group (green curves in A and B). In abiotic and heat killed OXA and NTA groups (black and blue curves), dissolved Fe^{2+} amount were identical to total aqueous Fe, suggesting rNAu-2 dissolution by these ligands. Dissolved Fe^{2+} in abiotic OXA and heat-killed OXA control groups gradually precipitated over time, but that in abiotic and heat-killed NTA groups increased over time. In contrast, in biotic OXA and NTA groups (red curves) aqueous Fe^{2+} rapidly decreased to a negligible level, while total Fe remained steady, suggesting that Fe(II)-OXA oxidized to form soluble Fe(III)-OXA. Lower levels of aqueous Fe^{2+} and total Fe in biotic NTA group than in abiotic and heat killed NTA groups (e.g., compare the red curves with black/blue curves)

suggest a stabilizing effect by biotic oxidation of Fe(II) in rNAu-2. Error bars are from two replicate experiments.

Figure 5. Nitrogenous gas production in bio-oxidized NTA, OXA, and no ligand group (16 day incubation). The majority of gas products were N₂, with small amounts of N₂O produced in NTA and no ligand group. NTA and OXA abiotic groups did not show N gas production with no nitrate reduction.

Figure 6. Chemical oxidation of Fe(II) in rNAu-2 by nitrite without the addition of ligand (a-c), in the presence of OXA(d-f) and NTA (g-i). The addition of OXA or NTA did not enhance significantly the rate of ferrous iron oxidation. Data points are experimental results, and error bars are from two replicate experimental tubes; solid lines are modeling results.

Figure 7. Initial pseudo-first-order rate constants (k) comparison between cell biotic oxidation and nitrite abiotic oxidation of Fe(II) in rNAu-2 with NTA, OXA or no-ligand in the beginning of the incubation. Nitrite was omitted in legend. Cell biological Fe(II) oxidation with or without the presence of organic ligands were much faster than that of nitrite abiotic Fe(II) oxidation.

Figure 8. Time-course changes of UV-vis spectra showing Fe-oxalate (260 nm, A, B, C) and Fe-NTA (258 nm, D, E, F) complexes. Abiotic and heat-killed OXA groups showed an absorbance peak at day 2 but disappeared since day 16. Abiotic, heat killed and biotic NTA groups all showed Fe-NTA absorbance peak from day 2 to day 60.

Figure 9. Interfacial electron transfer (IET) from Fe(II) rNAu-2 to Fe(III)-NTA, as evidenced by instantaneous jump of aqueous Fe²⁺ upon addition of Fe(III)-NTA (A) and a corresponding decrease of structural Fe(II) in rNAu-2 (B). Without addition of Fe(III)-NTA, no IET occurred and there was no aqueous Fe²⁺ or total Fe (aqueous symbols in A). In the second and third spikes, added Fe(III)-NTA complexes were only partially reduced, as evidenced by lower amount of Fe²⁺ production than the amount of total aqueous Fe (e.g., residual Fe(III)-NTA remaining). IET stopped at the third spike with only 0.1 mM Fe(III)-NTA reduced to Fe(II)-NTA. Error bars are standard deviation from two replicate experiments.

Figure 10. Time course (day 2, 16 to 60) changes of aqueous concentrations of Fe (A), Si (B), Mg (C), and Al (D) in biotic and abiotic incubations with rNAu-2 in the presence or absence of OXA and NTA. rNAu-2 and NO_3^- were omitted in group names in each group for succinctness.

Figure 11. Aqueous Fe/Si and Al/Si ratio from rNAu-2 dissolution for OXA group (A, C), and NTA group (B, D). Dashed line denotes corresponding stoichiometric ratio in NAu-2 structure. The dissolution of Fe, Si, and Al were incongruent under the effects of OXA and NTA for rNAu-2.

Figure 12. Dissolved Fe, Si, Al, Mg concentration of unreduced NAu-2 under the effects of OXA and NTA. Negligible amounts of Fe, Si, Al, and Mg dissolution were observed in OXA and NTA group for unaltered NAu-2.

Figure 13. FTIR spectra of Fe-Fe-OH-stretching and Fe-Fe-OH-bending bands in (a) unreduced NAu-2; (b) rNAu-2; (c) abiotic rNAu-2 + OXA; (d) abiotic rNAu-2 + NTA; (e) cell oxidized rNAu-2; (f) cell+OXA oxidized rNAu-2; (g) cell+NTA oxidized rNAu-2.

Figure 14. X-ray diffraction patterns for ethylene-glycolated, unreduced NAu-2, rNAu-2, rNAu-2 + OXA abiotic, rNAu-2 + NTA abiotic, cell oxidized rNAu-2, cell+OXA oxidized rNAu-2, and cell+NTA oxidized rNAu-2 after incubation of 60 days. Three broad peaks correspond to d_{001} , d_{002} , and d_{005} reflections of nontronite. T: talc; W: whewellite; F: ferrosilite.

Figure 15. X-ray diffraction patterns for NAu-2 sample with OXA under abiotic condition (ethylene-glycolated). Ferrosilite and Whewellite were detected in this sample.

Figure 16. SEM images of Strain 2002 after incubation for 60 days in OXA (A), NTA (B) and no-ligand group (C). No cell encrustations were found in NAu-2 experimental groups with or without the presence of organic ligands.

Figure 17. Scanning electron microscopic (SEM) images and energy dispersive spectroscopy (EDS) spectrum showing: (A) Formation of Whewellite in abiotic OXA

gorup, (B) Quartz formed in biotc OXA group, (C) Ferrosilite formed in abitoic OXA group.

Figure 18. A conceptual model for ligand-facilitated Fe(II) oxidation in the biotic NDFO process through interfacial electron transfer between rNAu-2 and Fe(III)-ligand complexes. Organic ligands promoted dissolution of Fe(II) from the rNAu-2 structure and formed Fe(II)-ligand complexes, and Fe(II)-ligand complexes were rapidly oxidized by strain 2002 through NDFO. Subsequently, aqueous Fe(III)-ligand complexes were reduced back to Fe(II)-ligand complexes by structural Fe(II) in rNAu-2 via a reversed IET, leading to structural Fe(II) oxidation.

TABLES

Table 1. Fe(II) concentration before and after bio-oxidation, bio-oxidation extent and rate

Ligand	Initial Fe(II)	Final Fe(II)	Bio-oxidation	Initial Bio-oxidation rate
	Conc. mM	Conc. mM	extent %	(1day) mM/day
OXA	4.926±0.215	0.841±0.015	82.927±0.316	1.854±0.068
NTA	4.893±0.121	0.735 ±0.005	84.979±0.101	2.475±0.013
None	5.083±0.111	2.633± 0.089	48.191±1.757	0.309±0.035

Bio-oxidation extent was calculated according to:

$$\text{Oxidation extent} = \frac{Fe(II)_{initial} - Fe(II)_{60days}}{Fe(II)_{initial}}$$

Bio-oxidation rate was calculated according to: Oxidation rate = $\frac{Fe(II)_{1day} - Fe(II)_{initial}}{\Delta \text{time}}$

Table 2. Calculated Fe(II) Speciation (Visual MINTEQ 3.1) in biotic OXA and NTA group

NTA		OXA	
Fe Species	Concentration (M)	Fe Species	Concentration (M)
Fe (NTA) ₂ ⁴⁻	2.09E-06	Fe-(Oxalate) ₂ ²⁻	1.53E-04
Fe ²⁺	9.53E-08	Fe ²⁺	6.15E-05
FeHNTA (aq)	1.06E-08	FeOH ⁺	1.19E-07
FeNTA-	7.76E-04	Fe-Oxalate (aq)	5.22E-04
FeOHNTA ²⁻	5.67E-08		

Table 3. Aqueous Fe²⁺ or clay structural Fe(II) oxidation rate by strain 2002 in NDFO

Fe Species	Initial Fe(II) Con. (mM)	Initial NO ₃ ⁻ Con. (mM)	Cells/ml	Buffer	Rate mM/d (first day)	Refs.
rNAu-2 (26%)	4.4	9	1 × 10 ⁸	PIPES	0.7	Zhao et al., 2015
rNAu-2 (27%)	4.3	9	1 × 10 ⁸	Bicarbonate	1.0	Zhao et al., 2015
Fe(II)-NTA	10	2.2	1 × 10 ⁸	PIPES	2.0	Weber et al., 2006b
FeSO ₄	3.5	2	6 × 10 ⁷	PIPES	3.2	Chen et al., 2018

FIGURES

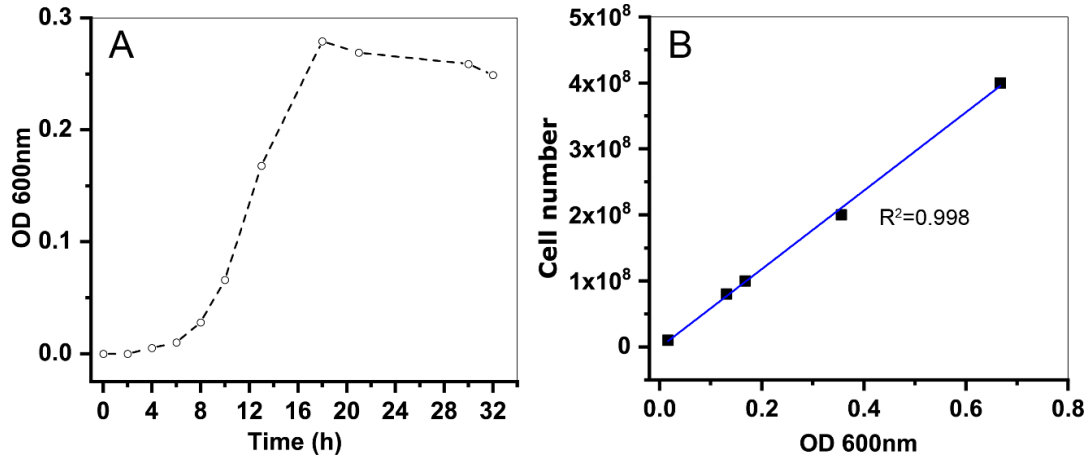


Figure 1

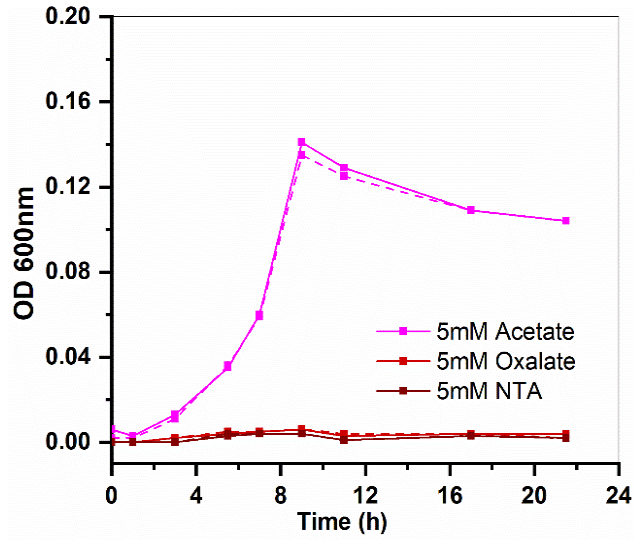


Figure 2

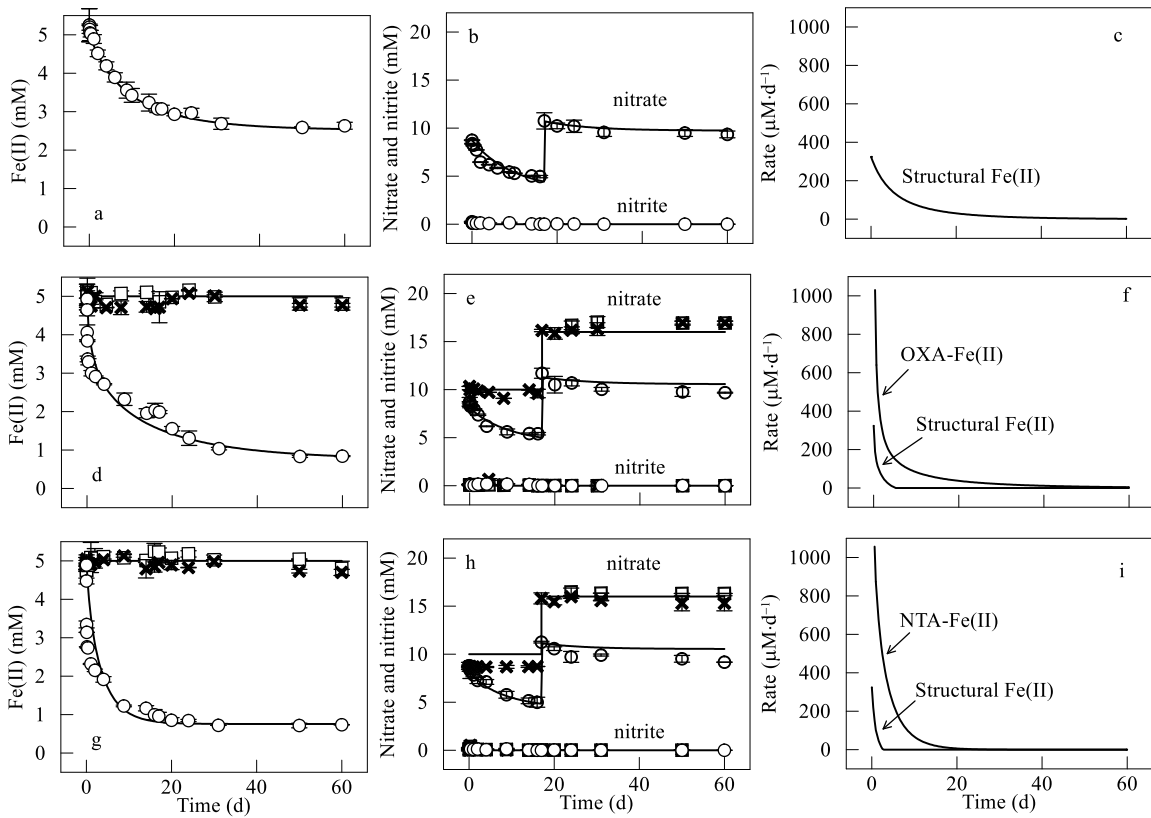


Figure 3

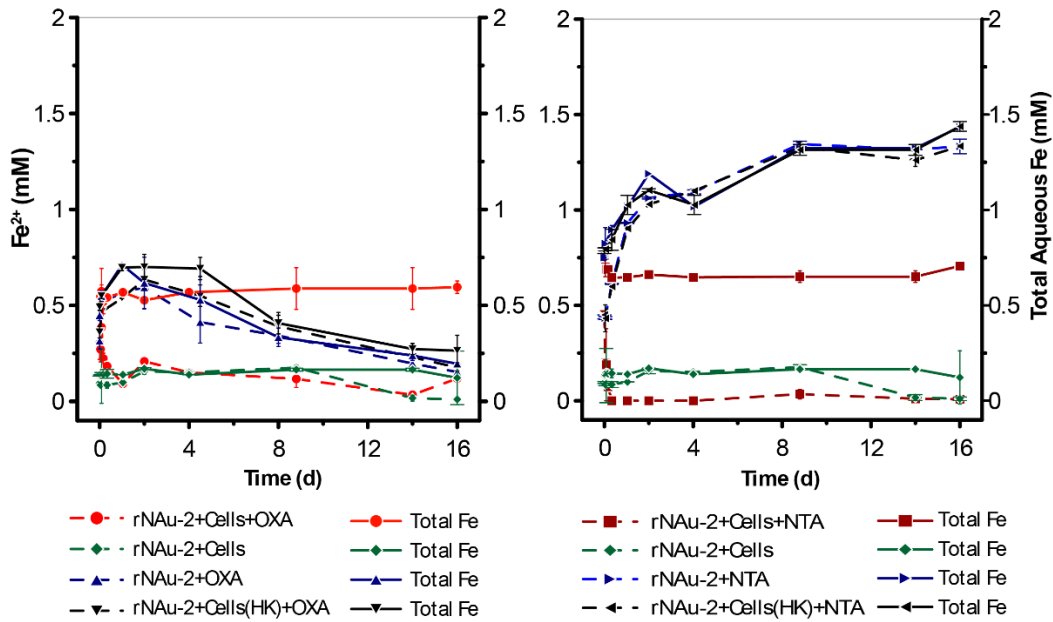


Figure 4

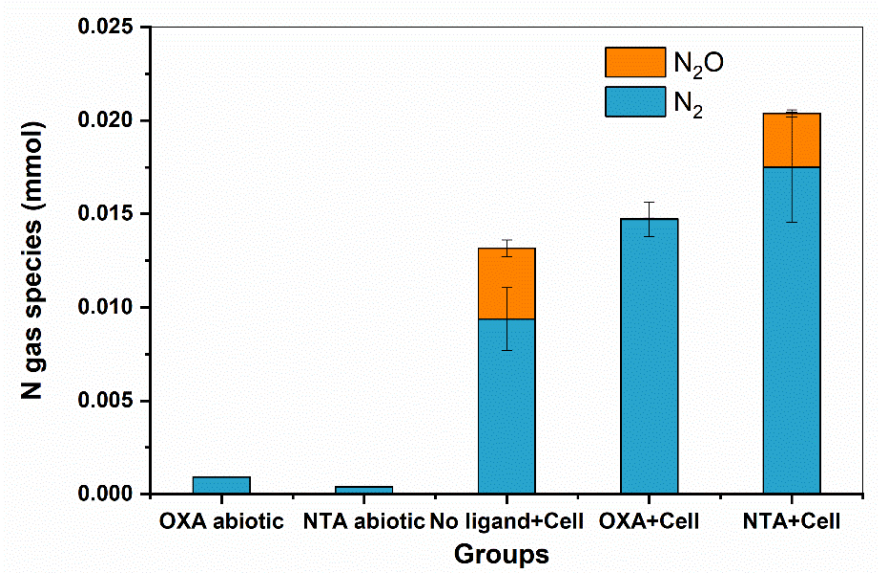


Figure 5

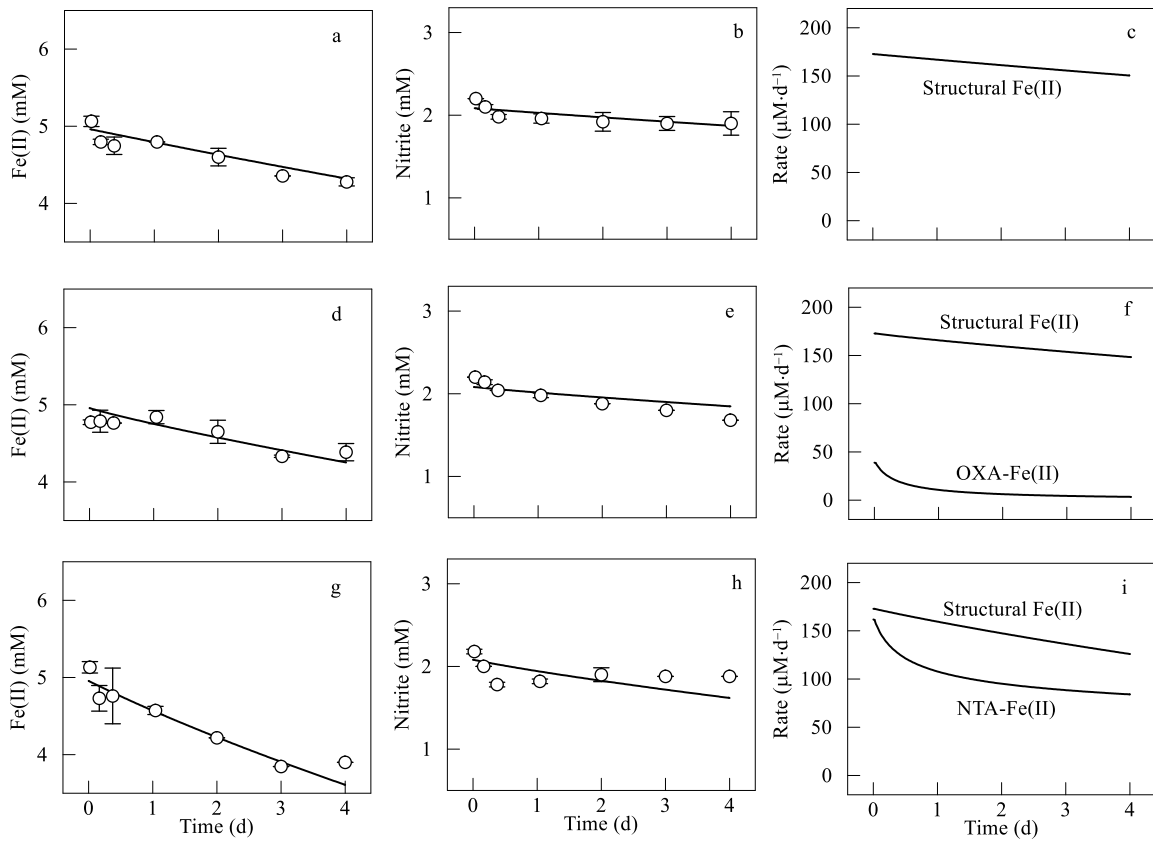


Figure 6

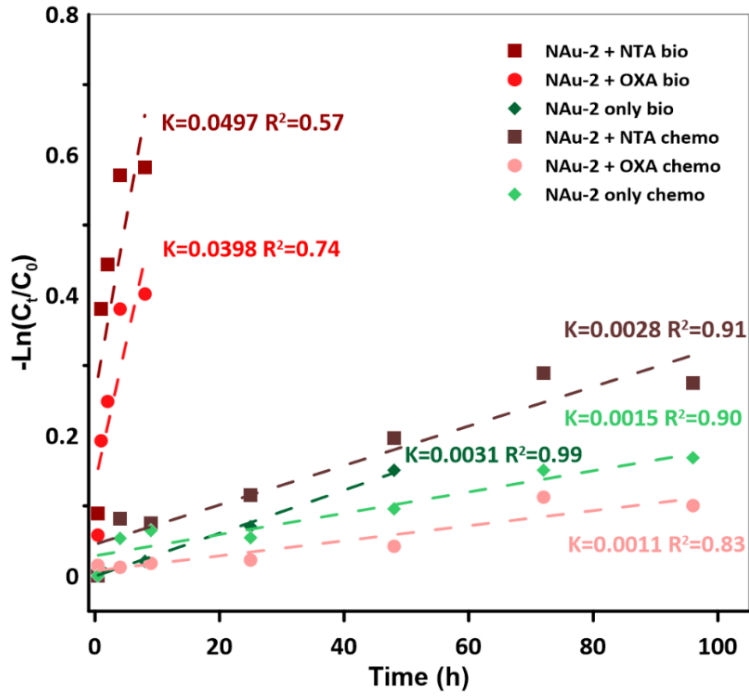


Figure 7

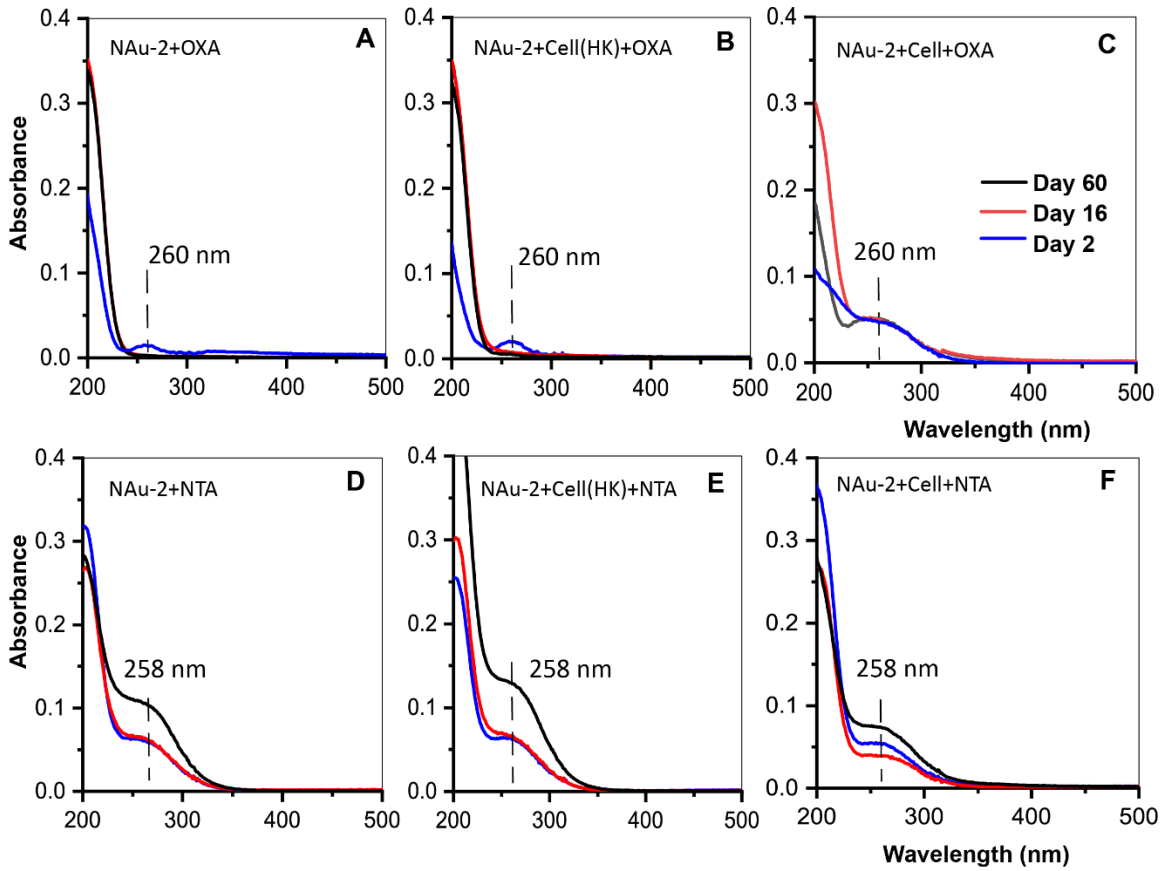


Figure 8

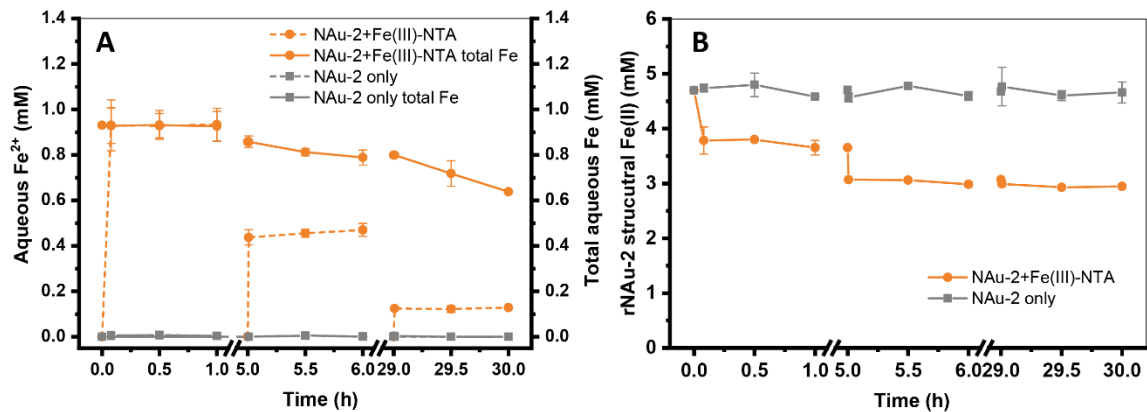


Figure 9

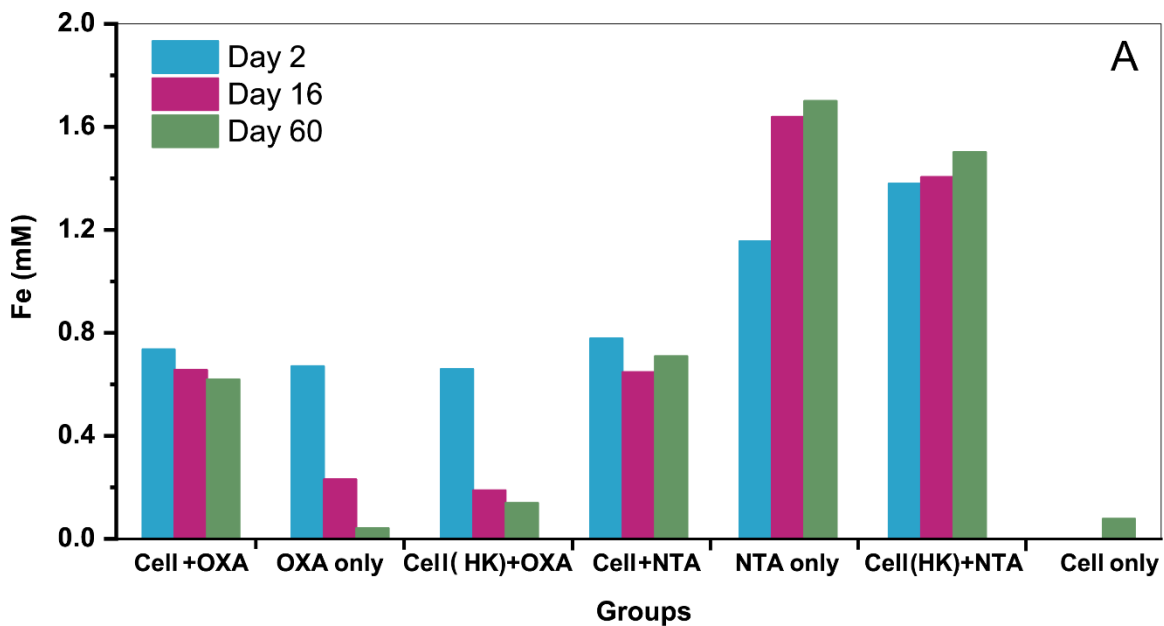


Figure 10A

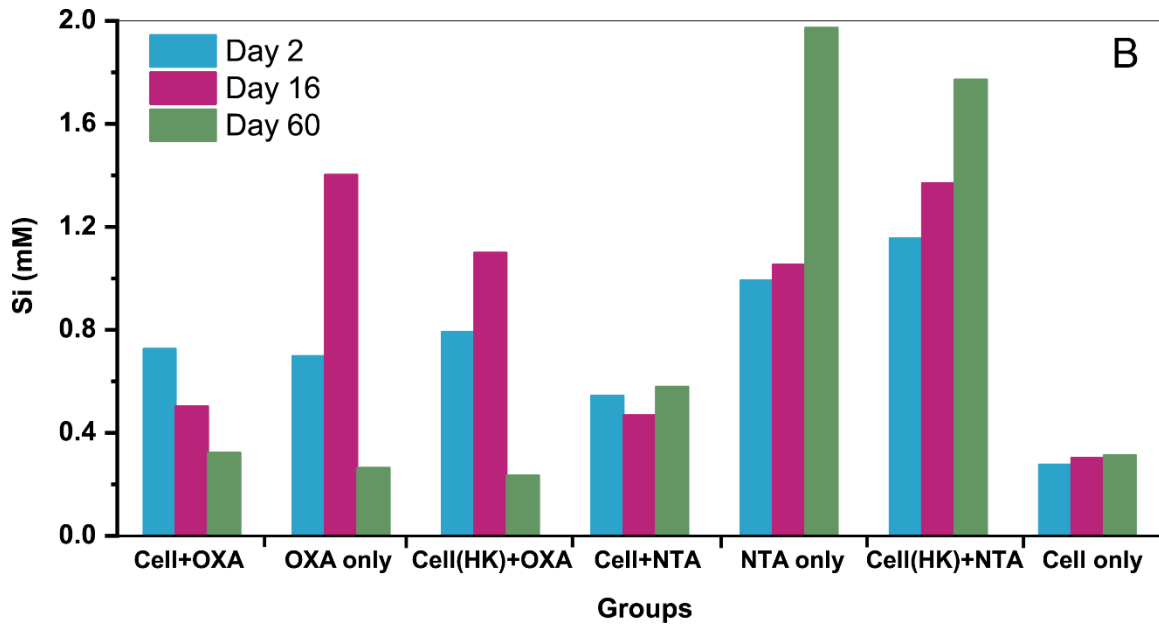


Figure 10B

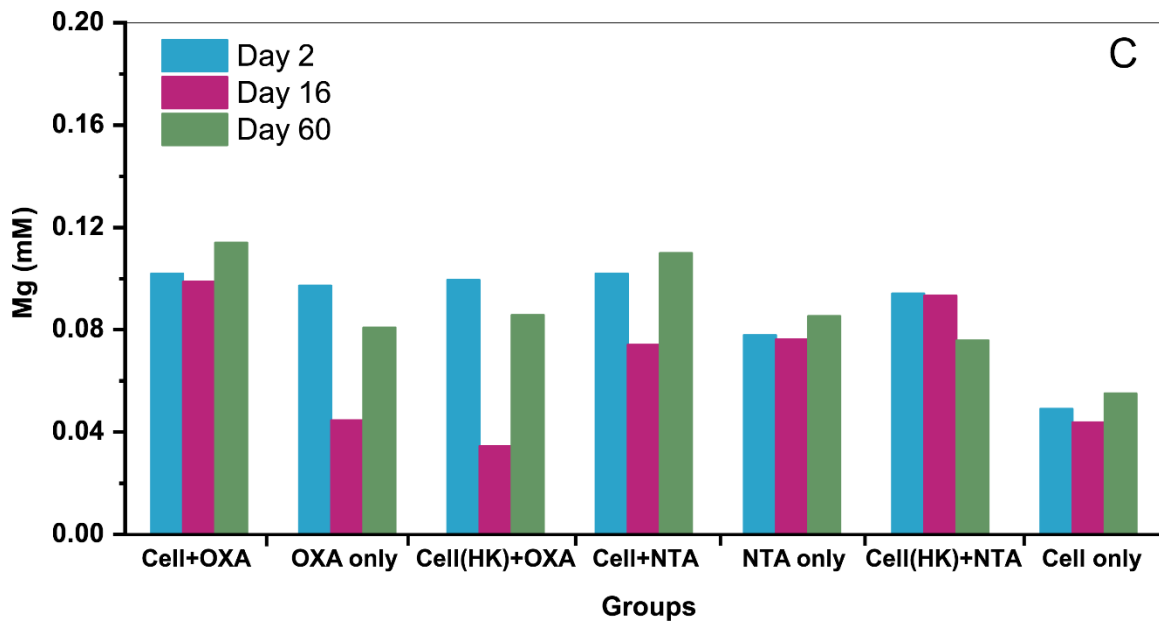


Figure 10C

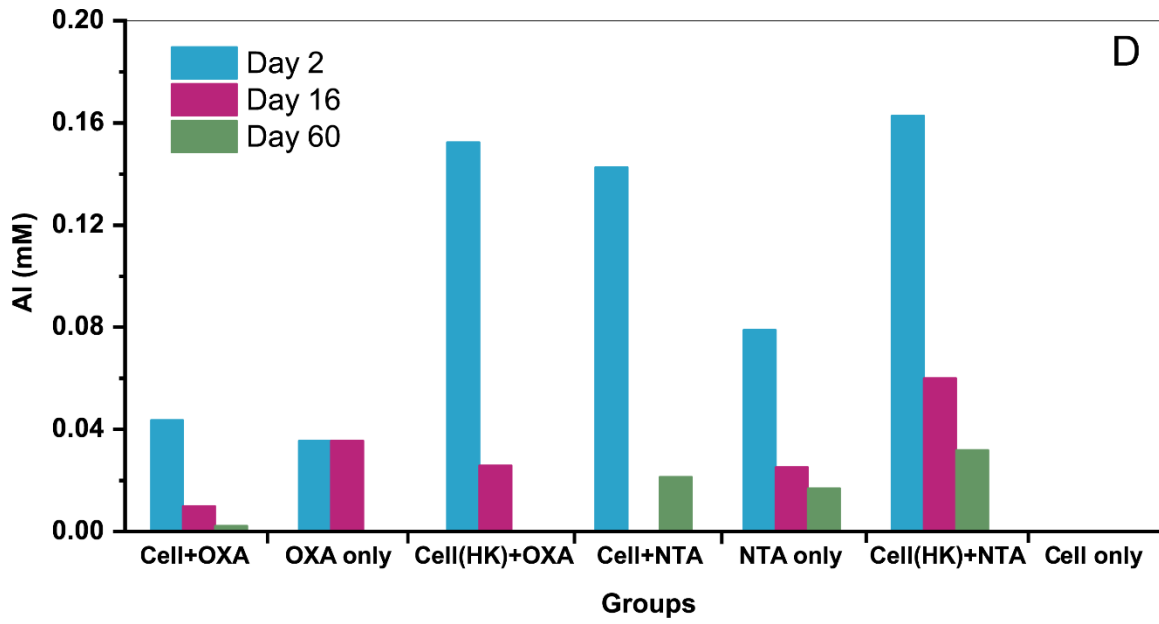


Figure 10D

Figure. 10

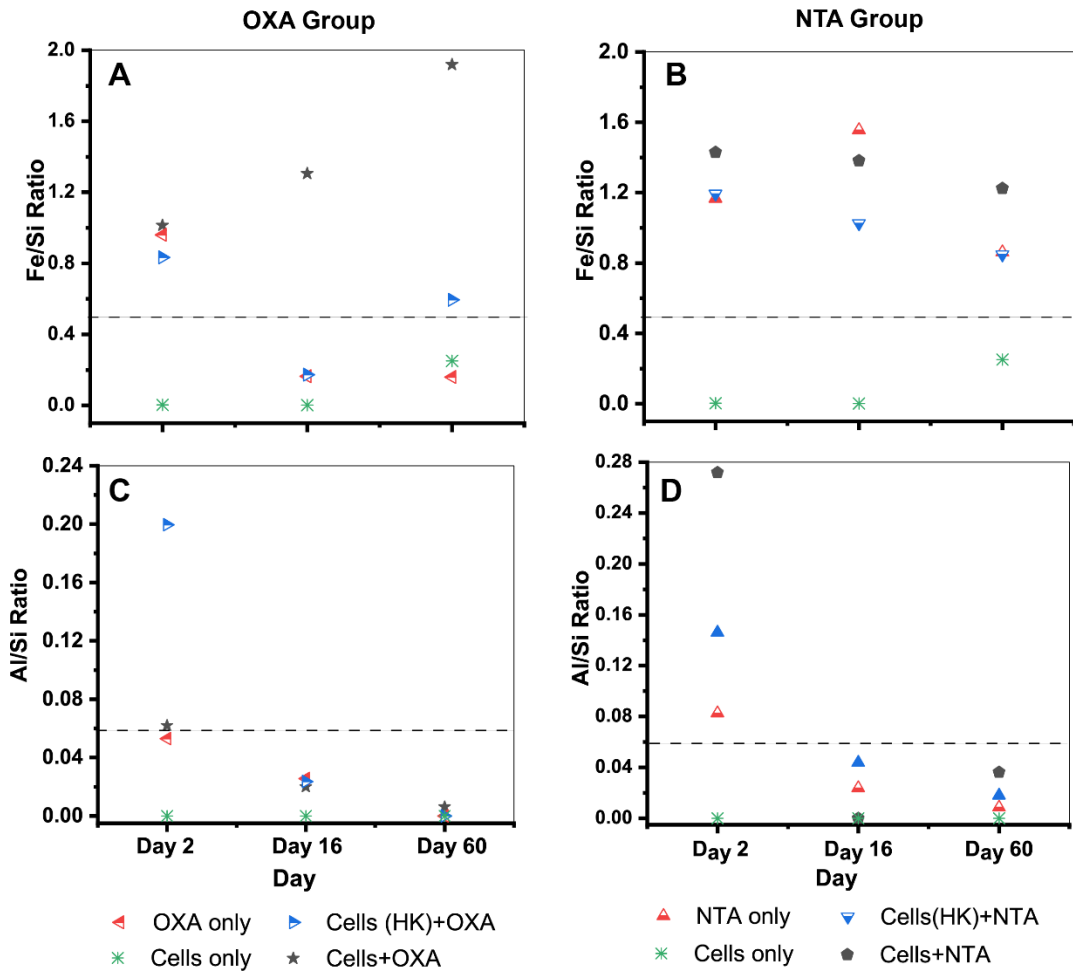


Figure 11

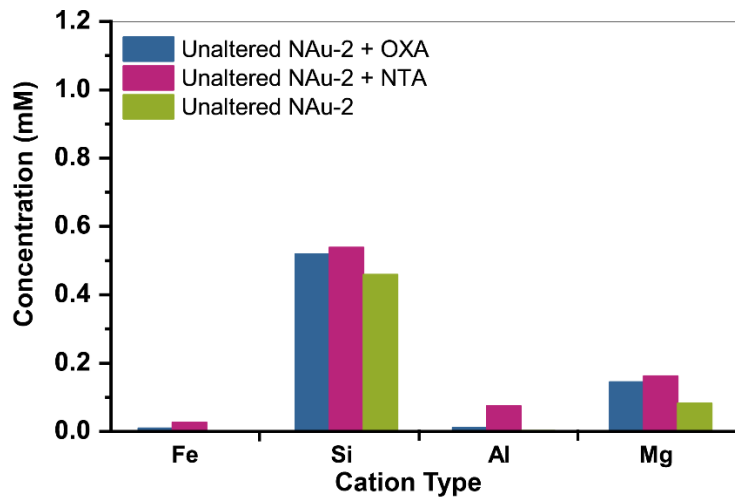


Figure 12

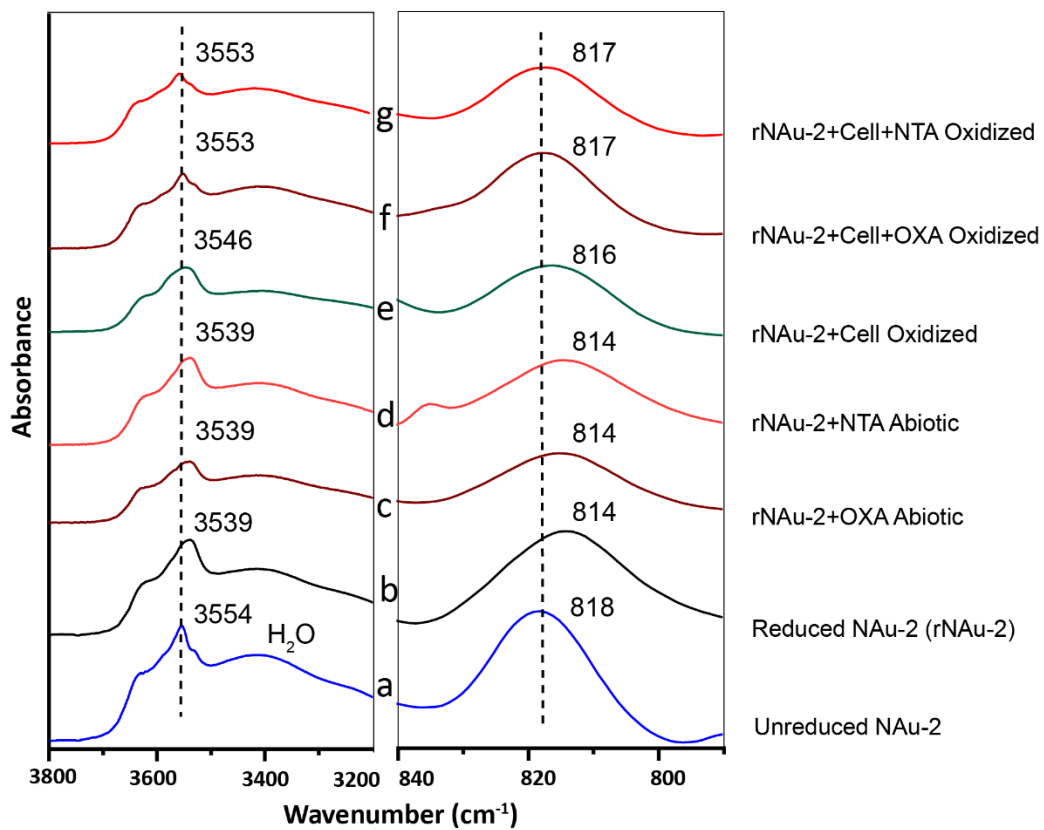


Figure 13

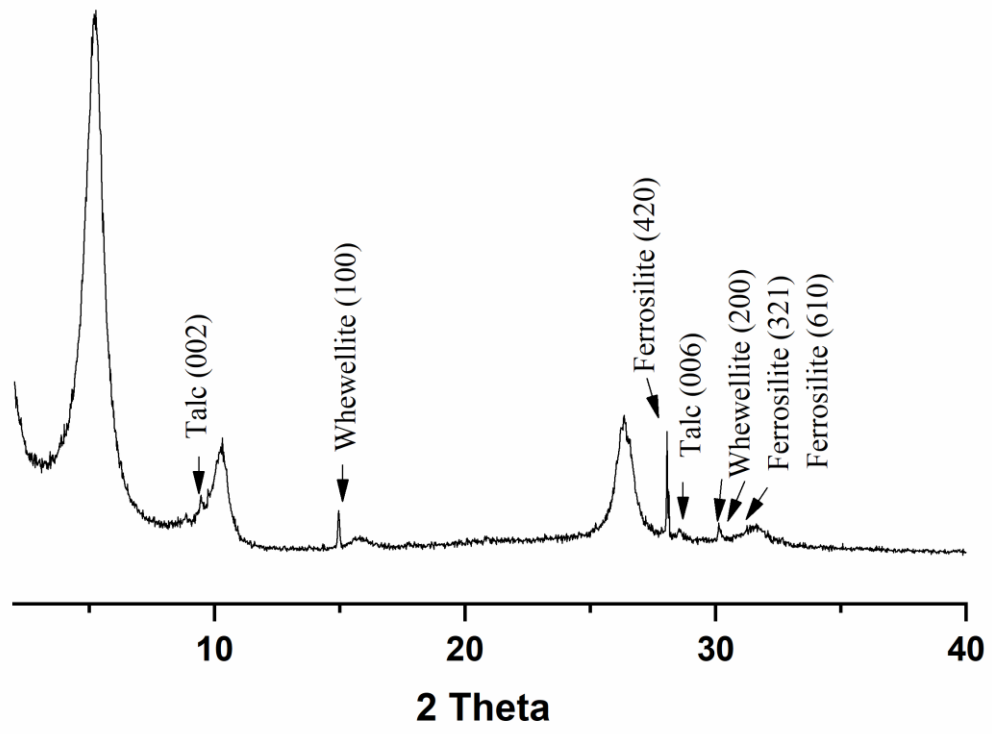


Figure 15

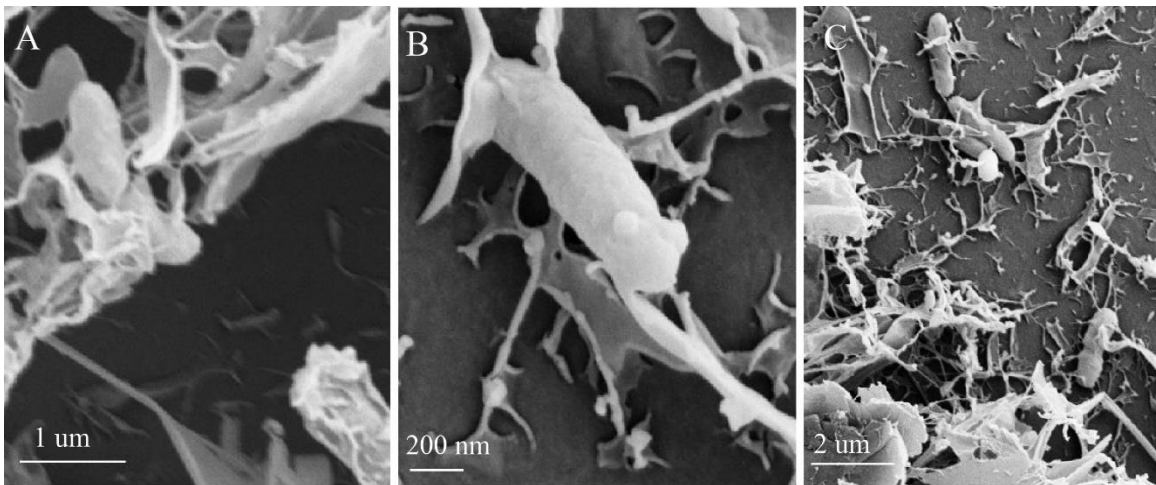


Figure 16

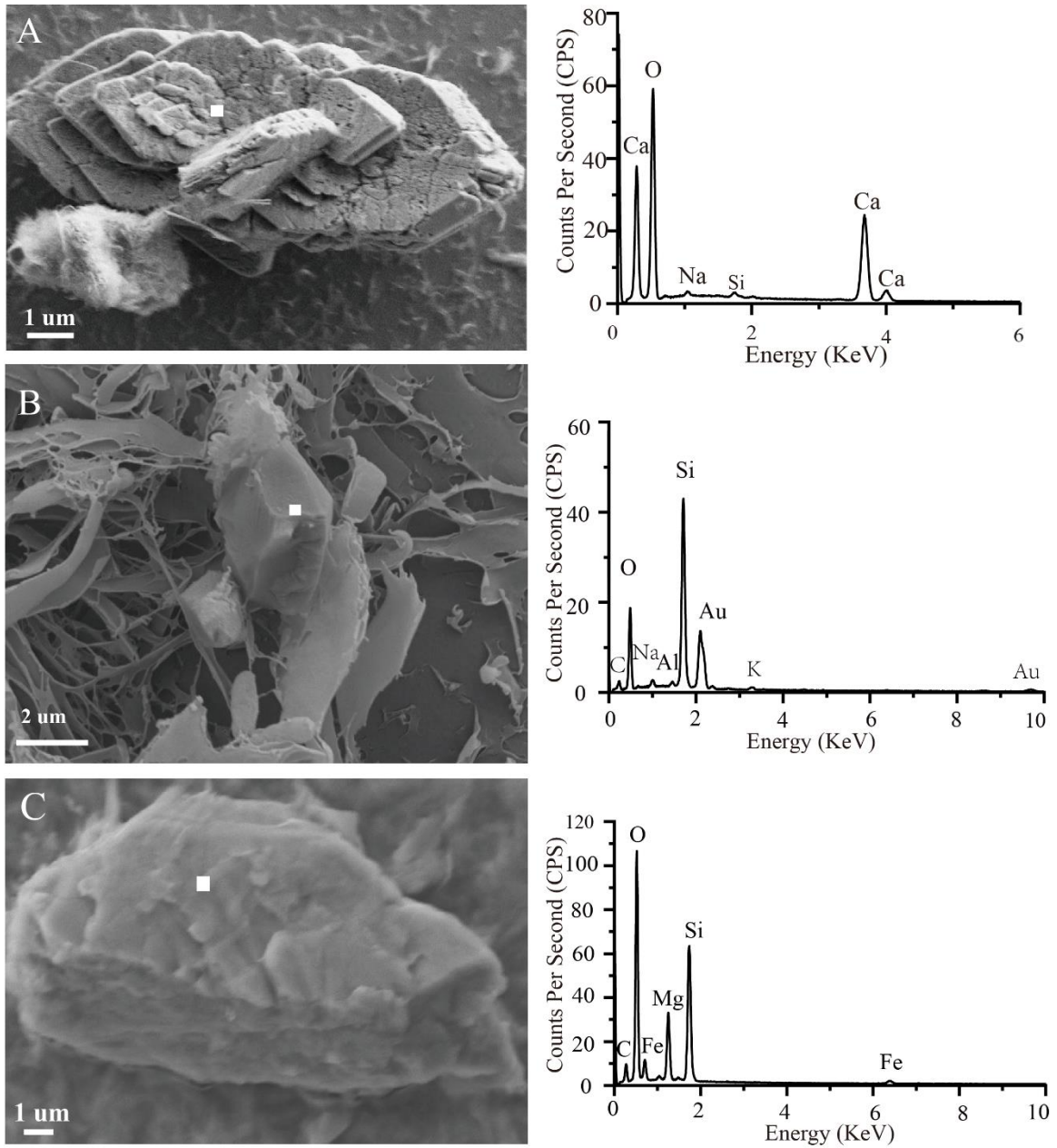


Figure 17

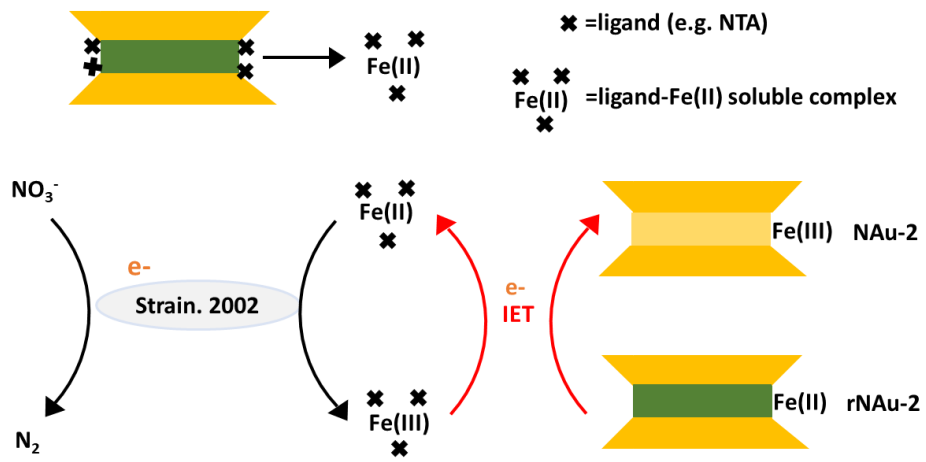


Figure 18